Bulletin of the New Zealand Society for Earthquake Engineering, Vol. 56, No. 4, December 2023

EARTHQUAKE DESIGN LOADS FOR RETAINING WALLS

John H. Wood[1]

(Submitted *August 2022*; Reviewed *December 2022*; Accepted *February 2023*)

ABSTRACT

Free-standing retaining walls are usually designed for earthquake loads assuming cohesionless backfill soil and using the Mononobe-Okabe method. This simple design approach has led to satisfactory performance and is supported by laboratory testing and analytical studies. For major wall structures there are a number of refinements to the method that should be considered. In the paper methods of assessing the influence on the earthquake loads of the flexibility of the wall, soil cohesion and ground water in the backfill are presented. Equations for predicting failure plane angles to allow a better assessment of the soil properties within the failure wedge are included. Procedures for estimating the outward displacement and the influence of passive resistance and wall geometry on the sliding resistance are discussed. Design charts are presented which allow the magnitude of these refinements to be rapidly assessed.

https://doi.org/10.5459/bnzsee.1618

INTRODUCTION

The behaviour of wall structures during earthquakes can be broadly classified into three categories related to the maximum strain condition that develops in the soil near the wall. The soil may remain essentially elastic, respond in a significantly nonlinear manner, or become fully plastic. The rigidity of the wall and its foundations will have a strong influence on the type of soil condition that develops.

Many low walls are of cantilever type construction. In this type of wall, lateral pressures from gravity and earthquake forces will often produce sufficient displacement within the wall structure and foundation to induce a fully plastic stress state in the retained soil. In rigid free-standing walls, such as gravity (e.g., mechanically stabilised earth and concrete block walls) counterfort walls and building basement walls, a fully plastic stress state may develop as the result of permanent outward movement from sliding or rotational deformations in the foundation. In cases where significant nonlinear soil behaviour or a fully plastic stress state occurs in the backfill soil during earthquake loading, the well-known Mononobe-Okabe, (M-O) method [1] can be used to compute earthquake pressures and forces acting on the wall.

Retaining structures that are not free-standing or have rigid foundations (piles or footings on rock or stiff soil) may not displace sufficiently, even under severe earthquake loading, for a fully plastic stress state to develop in the soil backfill. For these types of walls, it is important to estimate the displacements to check the applicability of the M-O method. It is more difficult to analyse these stiff walls but the earthquake loads can be satisfactorily estimated by interpolation between loads based on elastic rigid wall [2] and M-O theory.

The aim of the paper is to outline refinements that should be considered when estimating earthquake design soil pressures on major free-standing wall structures. The M-O analysis method is often used for wall earthquake deign and attention is focused on how, with a moderate increase in complexity, the wall stiffness and the foundation and backfill soil properties can be considered in more detail to reduce (or possibly increase) the earthquake forces calculated using the simplest form of the M-O equation. Charts are presented that allow the magnitude of these refinements to be rapidly assessed for design.

Topics discussed in the paper and their relevance to design based on the M-O analysis method are summarised below.

Failure Modes

Whether the failure of the wall occurs within the soil or within the wall structure has a bearing on the wall deformations and the applicability of the M-O method. Determining the failure mode is also important in deciding on the wall geometry, component strength and ductility required to limit damage to acceptable levels under the design earthquake loads.

Wall Flexibility

Charts that indicate the pressure reductions from wall and foundation deformations and indicate whether the M-O method can be used directly are presented (reproduced from [3]).

The influence of the depth of foundation soil below the wall on the earthquake induced pressures on the wall is assessed with reference to experimental results.

High Ground Accelerations

In high ground accelerations general failures may occur in the backfill soil slope and the conventional M-O equation does not have a solution when this occurs. A modification to the M-O method that considers the effects of strain localization in the backfill soil and the associated post-peak reduction in the shear resistance from peak to residual values along a previously formed failure plane is presented. The method results in a reduction to the size of the failure block and forces on the wall.

Generalised M-O

A generalised M-O analysis method is presented that considers, inclination of the wall-soil interface, backfill slope angle, surcharge on the backfill, tension cracks, wall-backfill friction and adhesion, cohesion and angle of shearing resistance of the backfill. An analytical expression for the critical inclination of the failure plane within the soil backfill is also presented. This allows the failure plane angle to be determined when either the backfill or residual soil has significant cohesion. Reductions in the M-O force may occur when the failure plane angle is predetermined by the boundary between the backfill and a surrounding soil with greater shear strength than the backfill.

[1] *Corresponding Author, Retired Civil Engineer, Lower Hutt, john.wood@xtra.co.nz (Life Member)*

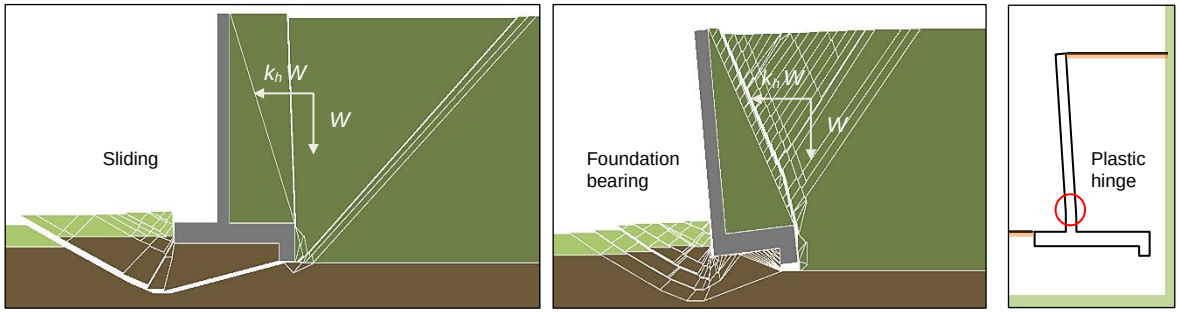

Figure 1: Failure modes reinforced concrete cantilever wall.

Outward Sliding

For high earthquake ground accelerations and walls with steep backfill slopes it will often be advantageous to design for permanent displacements from sliding and rotation of the wall arising from foundation soil deformation or ductility in the wall structure. The M-O analysis can then be based on the critical acceleration to initiate permanent displacement rather than the peak ground acceleration (PGA). An empirical equation is presented that can be used to estimate the outward displacement as a function of the ratio of the critical acceleration to the PGA.

The sliding resistance of cantilever and gravity walls is usually taken as the sum of the friction force on the base of the footing and the passive resistance on the effective toe depth of the wall. Values of the passive resistance of both a cohesionless and cohesive soil-wall interface under earthquake loading are presented that can be used to determine the passive pressure component of the resistance to sliding.

Wave Scattering

Seismic wave incoherence or scattering will reduce the average ground acceleration in the M-O failure block from the value estimated at the boundary beneath the wall. A relationship between this reduction and the wall height is presented.

Saturated Backfill

A procedure for calculating lateral earthquake pressures against a rigid wall from soil and water when the backfill soil is submerged, based on the M-O analysis procedure for unsaturated backfill, is presented. Modifications to the method for the case when the water level is below the top of the wall are discussed.

WALL FAILURE MODES

An important step in the design process for major walls is to identify the failure modes and to determine acceptable levels of damage under design level earthquakes. Possible failure modes for a reinforced concrete cantilever wall subjected to horizontal earthquake loads are shown in Figure 1.

The failure slip lines for both the sliding and foundation bearing modes shown in Figure 1 were calculated by the Limitstate:Geo (LS: Geo) software [4].

Of the three failure modes shown for the cantilever wall a sliding failure in the soil may be the preferred failure mode if the wall can move without causing damage to adjacent structures both in front of and above the wall. However, a particular issue is ensuring this type of failure is the most likely and it will usually be necessary to prevent other modes by using large overstrength factors for the resting forces which comprise both friction on the wall base and passive resistance at the foundation toe and shear key. With a shear key located at the rear of the wall foundation footing the failure will occur through the soil rather on the interface between the base slab and soil and the depth of the passive resistance surface will be at least the depth of the footing and shear key.

Slip lines below and in front of the wall indicate that the usual simplifying assumptions regarding the foundation resistance will only be approximate. For major walls it is best to investigate failures in the soil foundation using LS: Geo or equivalent software.

Foundation bearing type failures may result in excessive rotation of the wall that will be difficult to rectify. For this reason, they should be avoided. In many cases this can be achieved by using a foundation of conservative width.

Although plastic hinges in reinforced concrete cantilever stems can be designed to be ductile the associated cracking of the soil face of the stem may give rise to long term durability issues. Application of overstrength factors and a conservative estimate of the lateral loads on the stem will be required to limit crack widths to levels that are satisfactory for long term durability.

The overall stability of the wall in the surrounding geology and the influence of local ground topography should be part of the wall design investigation.

WALL FLEXIBILITY

In cases where significant nonlinear soil behaviour or a fully plastic stress state (active pressures) occurs in the backfill soil during earthquake loading the M-O can be used to compute earthquake pressures and forces acting on the wall. Walls that are restrained against displacement in the foundations and have very stiff structural elements can be designed using the rigid wall elastic theory [2]. Figure 2 compares the pressure distributions from M-O and rigid wall theory and illustrates the very large difference between the pressures that develop from flexible and rigid assumptions. Walls that have stiff elements and foundations that prevent significant translation or rotation under earthquake loads should be designed for pressures intermediate between the two limiting cases. Examples include basement walls and hydraulic structures. A basement wall example is illustrated in Figure 3.

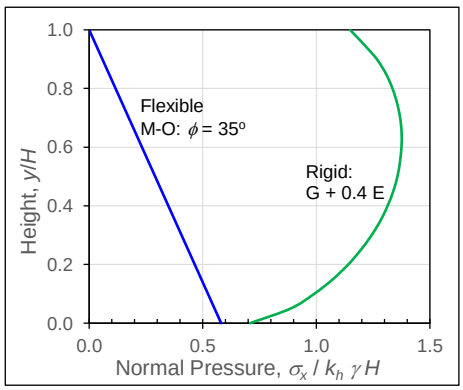

Figure 2: Earthquake plus gravity pressures.

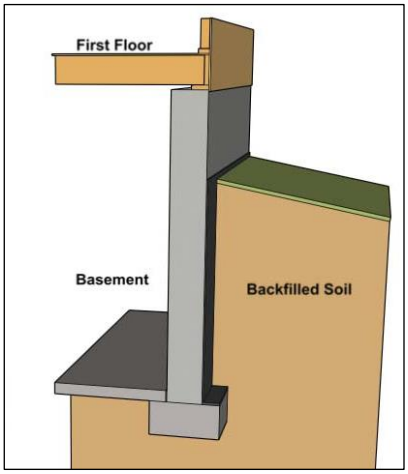

Figure 3: Basement stiff wall example.
From: https://designingyourperfecthouse.com/

Flexibility Parameters for Stiff Walls

Wood [3] carried out elastic finite element analyses (FEA) on cantilever walls that deform by both rotation about their base and flexure in the wall stem. The wall stiffness parameters were varied to produce pressure distributions under horizontal earthquake and gravity loads for walls that vary from rigid to sufficiently flexible for the M-O method to be applicable.

Tension pressures acting normal to the wall were eliminated. Both smooth and bonded soil-wall contacts were considered and backfill soils with a shear modulus both uniform over the height and with a linear increase from zero at the top of the wall to a maximum at the base were used.

Rectangular plain strain elements were used to model the soil, and beam elements to model the wall. Figure 4 shows details of the FEA model used for the analyses.

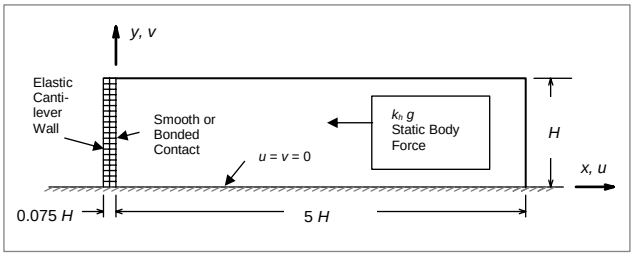

Figure 4: FEA model for flexural analysis of cantilever wall.

Results for the walls deforming in flexure were presented in terms of a flexibility parameter d_w defined by:

$$d_w = \frac{G\,H^3}{E_w I_w} \qquad (1)$$

Where G is the average soil shear modulus, H the height of the retained soil layer, E_w is the Young's modulus for the wall material and I_w the second moment of area of the wall per unit length.

Results for the walls deforming by rotation about the base were presented in terms of a flexibility parameter d_θ defined by:

$$d_\theta = \frac{G\,H^2}{R_\theta} \qquad (2)$$

Where R_θ is the rotational stiffness of the wall footing per unit length.

Pressure Distributions

The normal pressure σ_x on the wall deforming in flexure under horizontal earthquake load (uniform body force in the soil) in the soil with uniform soil elastic constants and for a smooth wall are shown in Figure 5. Corresponding pressure distributions for the rigid wall rotating about its base are shown in Figure 6. The pressure plots are presented in dimensionless parameters to enable them to be conveniently evaluated for any soil stiffness (shear modulus), soil unit weight, horizontal acceleration and wall height. For a given flexibility ratio d_w or d_θ, the normal pressures are dependent on the acceleration coefficient k_h, soil unit weight γ, and the height of the retained soil H, but are independent of the soil stiffness parameter directly.

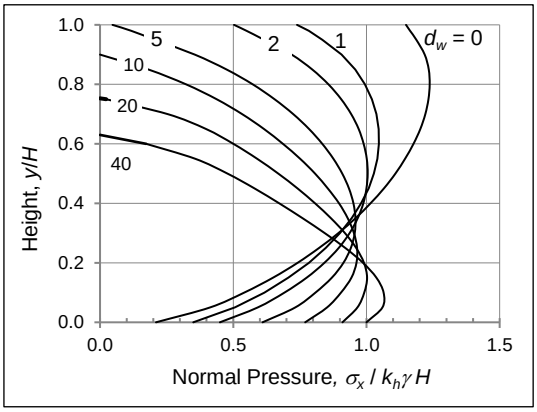

Figure 5: Normal pressure for flexural deformation.

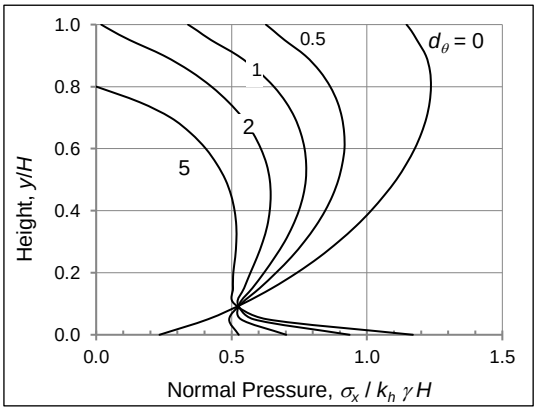

Figure 6: Normal pressure for base rotation.

Shears and Moments

The total force acting on the wall, V_b (or shear force at the base of the stem) and the bending moment at the base of the wall stem, M_b were obtained by integrating the pressure distributions.

Shears and moments per unit length for flexural deformation of the wall and the corresponding force actions for the wall deforming by base rotation are shown in Figures 7 and 8, and 9 and 10 respectively. The shears and moments shown in Figures 7 to 10 are plotted in dimensionless terms so that they can be used to evaluate solutions for any values of k_h, γ and H. A Poisson's ratio of 0.33 was assumed for the soil.

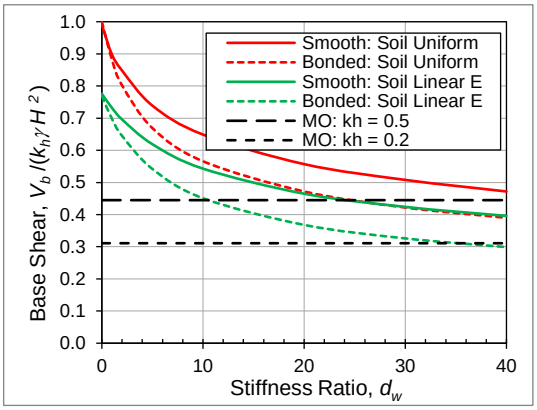

Figure 7. Base shear for flexural deformation.

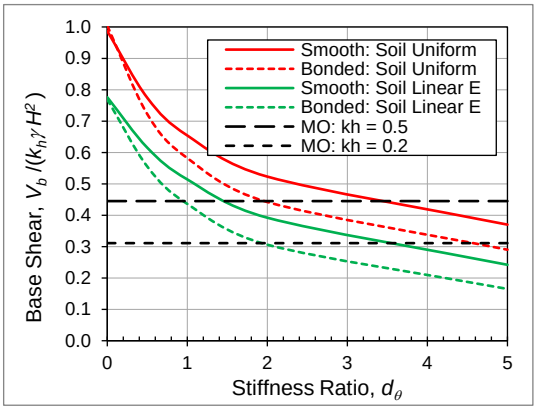

Figure 8: Base shear for rotational deformation.

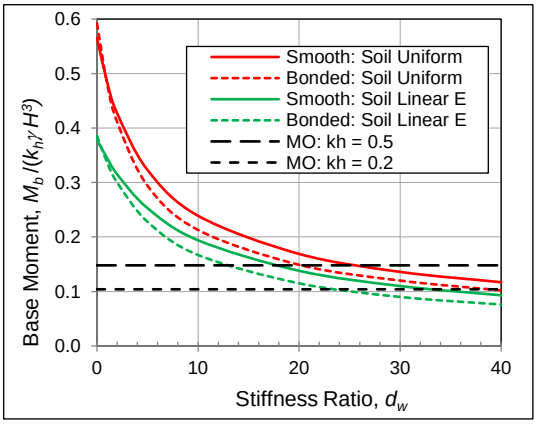

Figure 9: Base moment for flexural deformation.

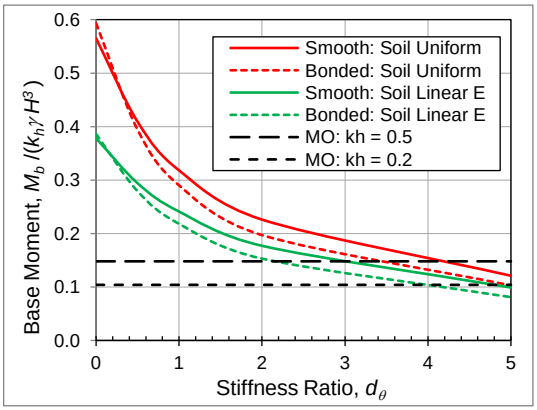

Figure 10: Base moment for rotational deformation.

Superimposed on the plots are M-O forces and moments calculated for a smooth wall assuming a soil friction angle ϕ = 35°. M-O values are plotted for acceleration coefficient values of k_h = 0.2 and 0.5. Since the M-O actions do not vary linearly with k_h and are independent of d_w and d_θ, they are drawn as separate horizontal lines for typical k_h values used in design.

Wall Deflections

Plots of the earthquake load component of the deflection at the top of the wall, u_t for both smooth and bonded walls with uniform and linearly increasing elastic constants with depth are shown in Figure 11. The corresponding deflections for the wall deforming by base rotation are shown in Figures 12. The factor required to express the deflections in dimensionless form includes the soil average shear modulus G in addition to k_h, γ and H. The top of the wall was assumed to be at the top of the soil layer.

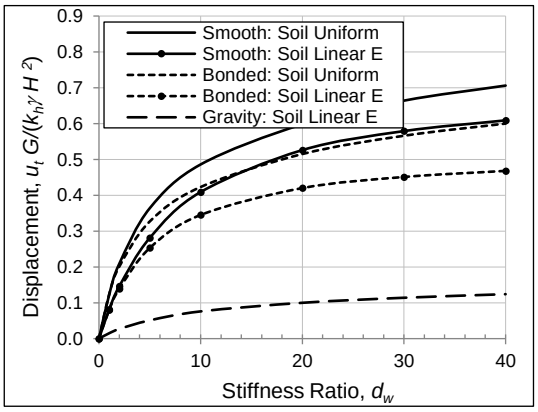

Figure 11: Top deflection: flexural deformation.

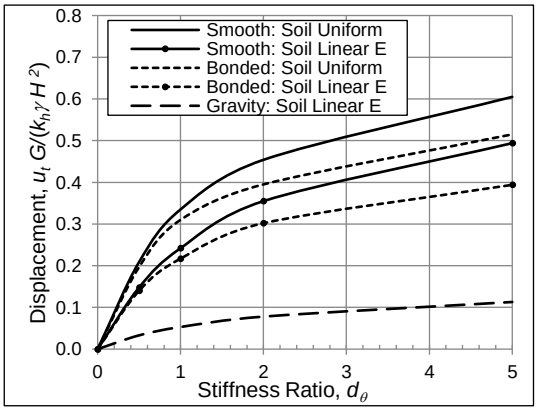

Figure 12: Top deflection: rotational deformation.

Gravity Actions

The shears and moments shown in Figures 7 to 10 do not include the components from gravity load in the backfill. In practical applications it is necessary to combine earthquake and gravity load pressures. Gravity pressures for rigid walls can be calculated by the conventional at-rest assumption (pressure coefficient K_o = 1- $\sin\phi$, where ϕ is the friction angle for the backfill soil) or by assuming elastic theory which gives K_o = $\nu/(1-\nu)$ where ν is the Poison's ratio for the backfill soil. For flexible walls, active Rankine pressure can be assumed but for stiff walls it is helpful to have results based on the elastic soil assumption consistent with the assumptions made for the earthquake pressures.

Gravity load shears and moments for flexural deformation in smooth and bonded walls and for soil with uniform and linearly increasing elastic constants with depth are shown in Figure 13. The corresponding base force actions for the wall deforming by base rotation are shown in Figure 14. Gravity load wall top deflections for the linear soil constants are shown in Figures 11 and 12. Deflections were approximately the same for both the linear and uniform soil assumptions. (Figures 5 to 14 have been reproduced from Wood [3].)

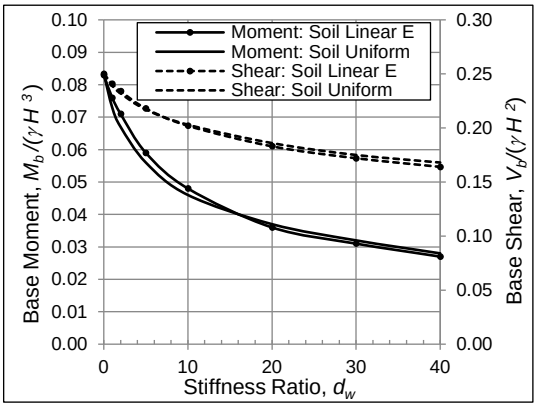

Figure 13: Gravity actions, flexural deformation.

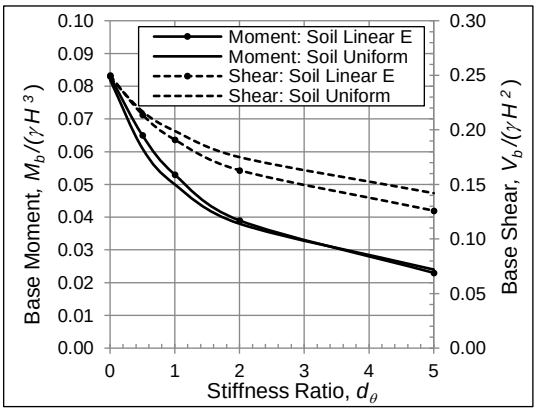

Figure 14: Gravity actions, rotational deformation.

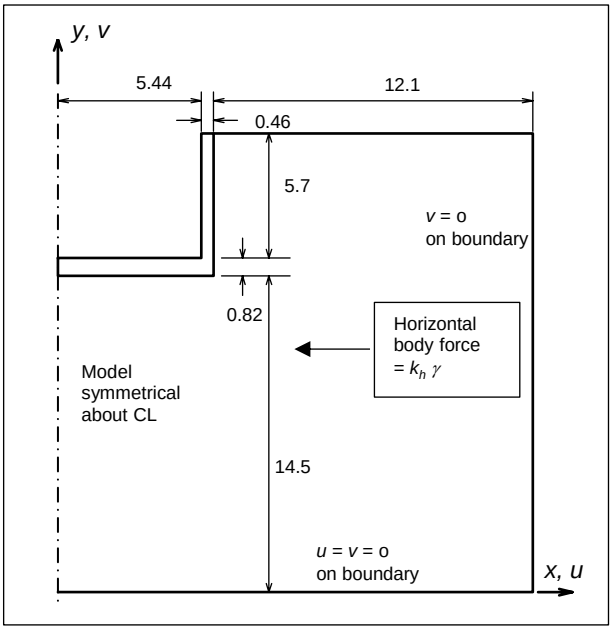

Figure 15: FEA model for U-wall with soil layer below wall.

Influence of Soil Layer below Wall

The FEA model used to calculate the earthquake response (see Figure 4) assumed that the wall and elastic soil backfill layer were founded on a rigid base. To investigate the influence of an elastic soil below the wall an analysis using the U-wall model shown in Figure 15 was undertaken as part of the present study. The dimensions were chosen to model the centrifuge experimental study reported by Mikola and Sitar [5] of a wall in cohesionless soil. The centrifuge model was a 1/36 scale model of a prototype wall and was subjected to a 36 g acceleration in the centrifuge.

Dimensions shown in Figure 15 are the prototype dimensions with the wall stem having a height of 5.7 m. The model wall was constructed of aluminium alloy and the properties of this material were used in the analysis of the prototype. The soil used in the model study was Nevada sand which is a fine uniformly graded angular sand. Material properties for the sand and wall structure based on values given in Mikola and Sitar [5] are summarised in Table 1. Earthquake loading was applied as a uniform horizontal body force acting within the soil. Analyses were carried out for the same uniform acceleration acting on the wall and for the case when the inertia force on the wall was zero. This later case was achieved in the analysis by assuming zero for the unit weight of the wall.

Table 1: Material properties for FEA of wall on soil layer.

Soil Properties		
Youngs modulus	E_s	100 MPa
Poisson's Ratio	ν_s	0.333
Unit weight	γ	16 kN/m^3
Initial friction angle	ϕ	36^o
Shear wave velocity	V_s	151.6 m/s
Layer depth below foundation	D_f	14.5 m
Backfill width	B_f	12.1 m
Wall Properties		
Youngs modulus	E_w	70,000 MPa
Unit weight	γ_w	26.5 kN/m^3
Stem height	H	5.7 m
Stem thickness	t_w	0.46 m
Stem MoI	I_w	0.00811 m^4
Wall stiffness parameter	d_w	12.2

Analyses were carried out for the model shown in Figure 15 and for a similar wall with the same stem height but with a rigid layer assumed to be located at the base of the stem. Analyses were undertaken for soil Youngs moduli of both 100 MPa and a reduced value of 50 MPa. Only elastic analyses were undertaken, and the reduced modulus value was used to model inelastic action expected in the soil under strong earthquake shaking. Wall stem stiffness parameters (d_w) were 12.2 and 6.1 for the 100 MPa Young's modulus and reduced modulus values respectively so the wall stem acted as a stiff wall at acceleration values up to 0.6 g.

The wall was modelled using a fine mesh to accurately capture the bending moments in the stem. Ten plane strain rectangular elements were used across the thickness of the stem and 80 elements over the height (elements size of 0.046 m wide x 0.071 m deep). Any tension that developed in the soil near the top of the wall was eliminated by a trial-and-error process with

the removal of soil elements in tension. Analyses were carried out for the soil assumed bonded to the wall and for the unbonded case or smooth wall. In this later case pinned rigid link elements were inserted between the wall stem and the soil.

Table 2 summarizes the analyses results for total shear force, base moment in the stem and deflection at the top of the wall stem for the case with the soil layer below the wall foundation and for no layer. For each of these two cases results are tabulated for inertia force acting on the wall structure and for no inertia force acting on the wall. The force actions and the displacements are presented in the dimensionless parameters defined in previous sections and are the average of the results for the bonded and smooth wall assumptions.

Table 2: Results with and without layer below foundation.

Parameter	No Layer		Layer	
	No Inertia	Inertia	No Inertia	Inertia
Shear force:	0.57	0.53	0.71	0.57
$V_b / (k_h \gamma H^2)$	(0.65)	(0.63)	(0.75)	(0.62)
Moment:	0.21	0.24	0.23	0.23
$M_b / (k_h \gamma H^3)$	(0.27)	(0.31)	(0.29)	(0.30)
Deflect. ratio:	0.10	0.12	0.25	0.27
δ / H %	(0.16)	(0.18)	(0.23)	(0.24)

The upper line for each parameter is for E_s = 100 MPa and the lower line with numbers in parentheses is for E_s = 50 MPa.

Results for no layer below the foundation are similar to those shown in Figures 7, 8 and 11. Minor differences arise from the differences in the length of the backfill layer between the wall and vertical boundary and other modelling details. For the case with the soil layer below the foundation the deflection at the top of the stem is increased by rotation in the joint of the stem with the wall base foundation.

Table 3 summarizes the percentage changes in the force actions and displacements between the case of no layer below the foundation and the case with the layer (average of the bonded and smooth wall results). A positive percentage indicates that the layer increased the force action or displacement. Again, the upper line for each parameter is for E_s = 100 MPa and the lower line with numbers in parentheses is for E_s = 50 MPa.

Table 3: Percentage change between layer and no layer.

Parameter	Percentage change	
	No Inertia	Inertia
Shear force:	23.5	9.0
$V_b / (k_h \gamma H^2)$	(15.0)	(-0.7)
Moment:	7.0	-2.4
$M_b / (k_h \gamma H^3)$	(0.4)	(-8.3)
Stem deflection:	50	39
Ratio: δ / H	(47)	(37)
Stem deflection	4.6	-2.0
No rotation at stem base	(-1.8)	(-8.1)

+ve change indicates layer increased force action or displacement.

The percentage changes for the force actions and stem displacements between the layer and no-layer cases is not very great with the differences between the base moments and displacement being less than 10%. Differences in the shear force are greater but still less than 10% for the analyses when the wall inertia was included.

Geometric details and the soil stiffness properties clearly influence the results, so it is not possible to make definite conclusions, but the example investigated suggests that the depth of soil below the foundation does not change the force actions and wall stem displacements that can be estimated using Figures 7 to 12 for the no-layer case by large amounts. This indicates that the simplified no foundation layer elastic analysis results can be applied to more complex foundation conditions. Precise force actions are not required as the elastic analysis should only be used as a guide to decide whether the wall behaves as a stiff wall and whether a more refined analysis is required.

Comparison of Elastic FEA and Experimental Results

The wall stem in the Mikola and Sitar [5] centrifuge U-wall model study was instrumented with strain gauges and pressure cells. Wall backfill and soil layers were instrumented with accelerometers and displacement transducers were used to measure the deformation of the wall stem. Ten earthquake recorded time-history shaking events were applied to the U-wall model with peak ground accelerations (PGA's) between 0.19 g and 0.64 g. Mikola and Sitar indicated that the frequency response of the pressure cells was inadequate to fully capture the dynamic pressures. The pressure cell data was only used to identify the shape of the dynamic earth pressures and the strain gauges were used to obtain the magnitude of the corresponding forces.

The Mikola and Sitar report [5] contained plots of the total dynamic bending moments in the wall stems estimated from the stem strain gauge readings. To obtain the dynamic component they subtracted the static component assuming at-rest pressures. Their main wall force and moment results are shown with the inertia effects of the wall removed from the dynamic component. Apparently, they estimated the wall inertia moments using accelerations recorded near the wall. From the elastic analyses described above it was clear that the dynamic component of moment in the wall stem was affected by both the inertia of the wall and the change in pressures acting on the wall. Pressures on the wall were reduced by the inertia of the wall so the overall change in stem base moment for the case of inertia included to the case with inertia excluded was not very large (see Table 2). This pressure modification from the wall inertia does not appear to have been considered in the results presented by Mikola and Sitar with their reduction to the total moments from wall inertia effects being much greater than indicated by the elastic analyses. Mikola and Sitar computed the dynamic force on the wall from the dynamic moments by assuming that the pressure force was of a triangular shape (indicated by the pressure cells) with the maximum pressure at the base of the wall. Any error in the moments would therefore have been transferred to their dynamic force results.

Because of the uncertainty in the wall inertia moments, the comparison between the elastic analyses and centrifuge experimental results in the present study was only made in detail with the wall inertia included results. Figures 16, 17 and 18 show comparisons between the elastic and experimental results for stem base bending moment, wall stem pressure force and stem top deflection respectively. The elastic analyses results are for the average of the bonded and smooth wall cases. To be consistent with the Mikola and Sitar notation the force on the wall is shown as the dynamic force component ΔK_{AE}. This dynamic component is defined as:

$$\Delta K_{AE} = 0.5(K_{AE} - K_o)\gamma H^2 \qquad (3)$$

Where K_{AE} is the total dynamic force coefficient (including gravity) and K_o the at-rest force coefficient. Mikola and Sitar calculated a dynamic moment component defined by:

$$\Delta M_{AE} = \frac{1}{6}\Delta K_{AE}\,\gamma H^3 \qquad (4)$$

The moment results shown in Figure 16 for the wall inertia excluded case are as plotted by Mikola and Sitar. The results for the included inertia case were derived from intermediate results given in Mikola and Sitar for the total moment and static at-rest component (no inertia component subtracted). There is a large difference between these sets of results and this is inconsistent with the elastic analyses that show only a minor difference. The experimental results with wall inertia included are in reasonable agreement with the elastic analyses results with E_s = 50 MPa. For PGA's less than 0.3 g the agreement is rather better for E_s = 100 MPa suggesting nonlinear soil response at larger PGA's.

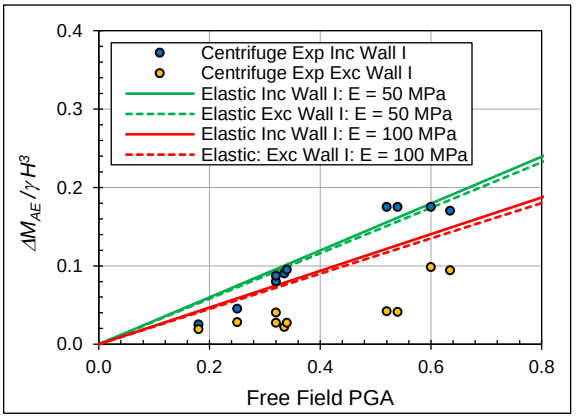

Figure 16: Moments experimental and elastic analysis.

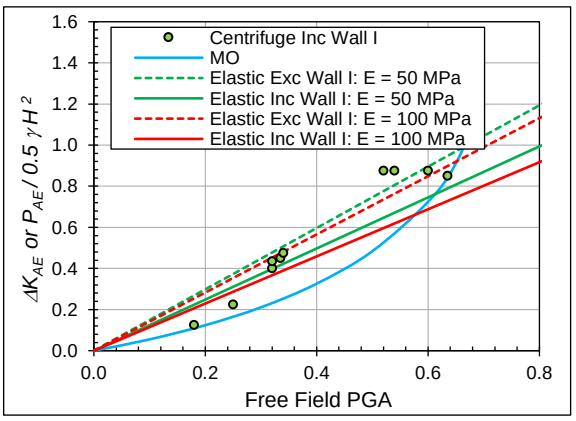

Figure 17: Wall force experimental and elastic analysis.

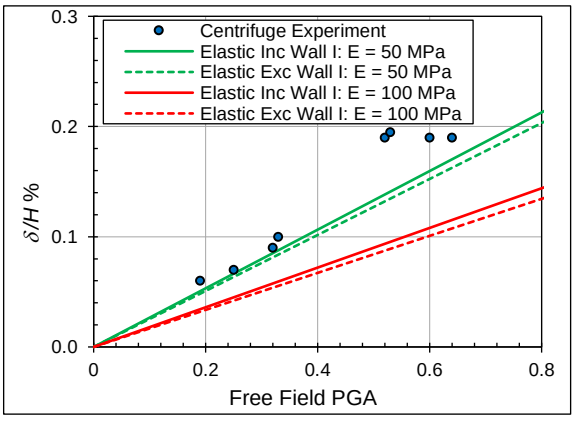

Figure 18: Wall top displacement experimental and elastic analysis.

The experimental dynamic force results plotted in Figure 17 were calculated from the experimental base moments (excluding the wall inertia) using the relationship given in Equation 4 but with the 1/6 factor taken as 1/5. This modification was based on the elastic analyses results which indicated that the pressure distributions were only approximately triangular. The M-O curve shown in the figure is based on a soil friction angle of 36° and a soil-wall interface friction of 18°. No wall inertia effects have been included in the M-O analysis. Figure 17 shows reasonable agreement between the experimental dynamic forces on the wall and the theoretical elastic and M-O results over the PGA range investigated (wave scattering effects could have reduced the experimental results by up to 10%). This interpretation differs from Mikola and Sitar who considered that the experimental results (with wall inertia effects removed) showed lower dynamic forces than those predicted by the M-O and other theories. They supported this conclusion with a dynamic inelastic analyses using the FLAC analysis software [6].

Experimental dynamic (transient) displacement ratios for the top of the wall stem shown in Figure 18 are as presented by Mikola and Sitar [5]. These ratios suggest that the active pressures developed in the backfill at PGA's greater than about 0.5 g. Up to this acceleration level the backfill will be essentially elastic with dynamic forces on the wall stem greater than indicated by the M-O analysis.

M-O FORCE AT HIGH GROUND ACCELERATIONS

For a cohesionless backfill the M-O active earthquake pressure force P_{AE} on the back face (virtual or actual) of is given by:

$$P_{AE} = 0.5\,K_{AE}\,\gamma H^2 \qquad (5)$$

Where K_{AE} is the active earthquake pressure coefficient, γ the unit weight of the soil and H the total vertical height of the soil on the back face (or virtual back face). K_{AE} is given by:

$$K_{AE} = \frac{\cos^2(\phi+\beta-\theta)}{\cos\theta\,\cos^2\beta\cos(\delta+\theta-\beta)\left[1+\sqrt{\frac{\sin(\phi+\delta)\sin(\phi-\theta-i)}{\cos(\delta+\theta-\beta)\cos(\beta+i)}}\right]^2} \qquad (6)$$

Where ϕ is the soil friction angle; β the wall inclination (positive in a clockwise direction from the vertical); δ the mobilized interface friction angle assumed to act at the back of the wall; i the soil backslope angle (from horizontal); and θ the seismic inertia angle given by:

$$\theta = tan^{-1}\left[\frac{k_h}{1-k_v}\right] \qquad (7)$$

The failure plane angle, α is given by:

$$\cot(\alpha - i) = -\tan(\phi+\delta+\beta-i) + \sec(\phi+\delta+\beta-i)\sqrt{\frac{\cos(\beta+\delta+\theta)\sin(\phi+\delta)}{\cos(\beta-i)\sin(\phi-\theta-i)}} \qquad (8)$$

Limiting Force Coefficient

When $\phi-\theta-i<0$ Equation 6 does not have a solution because the term within the square root part of the denominator becomes negative. K_{AE} reaches a maximum large value when $\phi-\theta-i=0$.

An infinite slope subjected to horizontal earthquake acceleration fails when $tan^{-1}(k_h) = \phi - i$ or when $\theta = \phi - i$. For example, if ϕ = 35° and i =30°, then θ = 5° giving k_h = 0.087. Assuming the friction angle on the wall-soil interface = 17.5° gives a maximum value of K_{AE} = 0.82 at the point of insipient failure of the backfill slope. At higher values of k_h shallow failures will tend to form in the surface of the backfill. It is unlikely that K_{AE} will increase significantly above its maximum value when this occurs. A plot of the maximum K_{AE} and slope

angles versus the earthquake acceleration coefficient is shown in Figure 19 for $\beta = \delta = k_v = 0$.

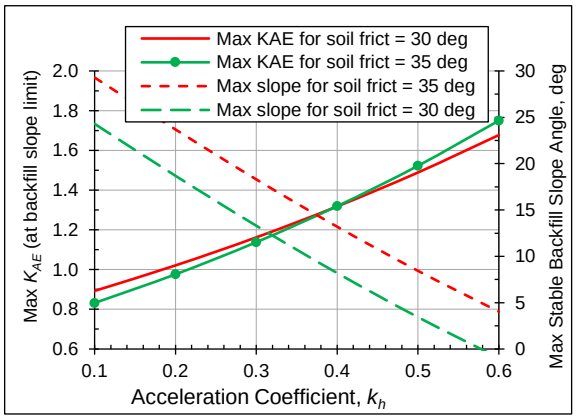

Figure 19: Maximum K_{AE} and stable backslope angles.

Reduction in Wall Pressures from Strain Localisation

Koseki et al [7] have proposed a modified pseudo-static and limit-equilibrium approach to evaluate active earth pressure at high seismic load levels. Their method is similar to the M-O method but considers the effects of strain localization in the backfill soil and the associated post-peak reduction in the shear resistance from peak to residual values along a previously formed failure plane. The proposed method results in a reduced and probably more realistic size of the active failure zone in the backfill soil at high seismic load levels compared to that predicted by the M-O method. The method is referred to below as the Failure-Plane method.

Koseki et al [7] indicated that based on results from a series of plane strain compression tests on dense sands and gravels, that the relative displacement in the direction parallel to the shear band which is sufficient to reduce the mobilized shear resistance from the peak to the residual angle value is about 5 to 10 times the mean diameter D_{50}. Koseki et al also stated that from dynamic centrifuge tests on retaining wall models, Bolton and Steedman [8] showed that the shear resistance angle mobilized along a failure plane, dropped from 50° to 33° by a relative displacement of the order of 10 times the mean particle diameter. They suggest that in full-scale field cases the drop of soil shear strength from the peak to residual values is likely to occur rapidly under earthquake loading. Further, the amount of outward wall displacement to trigger the active failure of the backfill associated with the mobilization of the peak friction angle in the shear band is small; for a wall rotating about its base, the outward displacement at the wall top is about 0.1 % of the wall height from the at rest condition. Therefore, the active failure in the backfill may occur under earthquake accelerations well below the level to cause ultimate failure by excessive wall deformation.

To implement the Koseki et al Failure-Plane method it is necessary to compute the active earthquake pressure coefficient for a known failure plane. They derived the following equation for this calculation:

$$K_{AE} = \frac{cos\,(\alpha-\phi)(1+tan\beta tan\alpha)(1+tan\beta tani)(\tan(\alpha-\phi)+ tan\theta)}{\cos(\alpha-\phi-\beta-\delta).(\tan\alpha-tan\,i)} \quad (9)$$

The Failure-Plane method is best described by working through the following example. For simplicity k_v, β, i and δ are assumed to be zero (vertical smooth wall with level backfill surface). The backfill peak and residual friction angles are assumed to be 45° and 35° respectively. Figure 20 shows the M-O active pressure coefficient, K_{AE} for these friction angles and for 40°, the average of the two values, as a function of the horizontal acceleration coefficient.

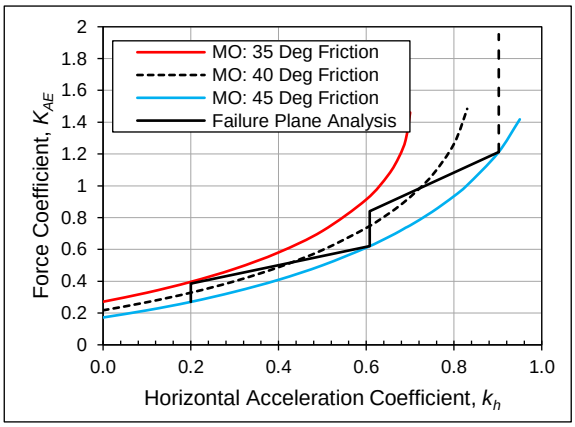

Figure 20: Failure-Plane analysis example.

The zig-zag straight lines lying between the M-O solutions for 45° and 35° is the Failure-Plane solution. The steps required to develop this solution are as follows:

a. The active pressure state is assumed to develop at a k_h value of 0.2. From a M-O analysis the corresponding active pressure K_{AE} = 0.27 and the failure plane angle 59.8°.

b. A failure plane develops with a residual friction of 35°. From Equation 9, K_{AE} increases to 0.385 as the sliding movement develops on the failure plane. (Vertical line in Figure 20 at k_h = 0.2.)

c. When the k_h value increases to a value of 0.608, application of Equation 9 for the residual friction gives K_{AE} = 0.622. Application of the M-O equation using the peak friction of 45° gives the same K_{AE} value. It is then assumed that a new failure plane develops at an angle of 38.5° as given by Equation 8 (M-O failure angle equation). Using the new failure plane angle and the residual friction in Equation 9 shows that the K_{AE} value increases to 0.841. This increase is represented by the vertical line in Figure 20 at k_h = 0.608. Sliding on the initial failure plane of 59.8° is indicated by the sloping straight line between k_h values of 0.20 to 0.608.

d. When k_h increases to a value of 0.902, application of Equation 9 for the residual friction gives K_{AE} = 1.212. Application of the M-O equation using the peak friction of 45° gives the same K_{AE} value. It is then assumed that a new failure plane develops at the angle of 15.9° as given by Equation 8. Using the new failure plane angle and the residual friction in Equation 9 shows that the K_{AE} value increases to 1.953. This increase is represented by the vertical dashed line in Figure 20 at k_h = 0.902. Sliding on the old failure plane of 38.5° is indicated by the sloping straight line between k_h values of 0.608 to 0.902.

Figure 21 shows the intersection of the active pressure lines, based on the residual friction of 35°, for failure plane angles of 59.8° and 38.5° (Equation 9) with the M-O solution based on the peak friction angle of 45°. These intersection points indicate the k_h values at which the new failure planes develop (the initial failure angle of 59.8° changes to an angle of 38.5° and this angle changes to 15.9°. Plotting the failure plane solutions (K_{AE} versus k_h) is a convenient method of determining the k_h levels at which the failure plane slope changes.

The Failure-Plane analysis indicates that the K_{AE} pressure coefficient might be significantly lower than computed by M-O using the residual friction angle. Using an average of the peak and residual friction angle in an M-O analysis would give a more correct estimate of K_{AE} in strong earthquake accelerations

than using the residual friction as indicated by the M-O curve in Figure 20 for a friction angle of 40°.

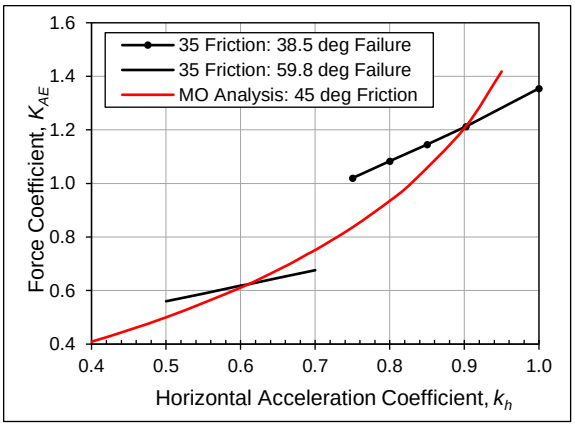

Figure 21: Intersection of residual friction failure planes with M-O peak friction angle.

Failure plane development was monitored by Watanabe et al, [9] in a series of shaking table tests on 530 mm high model gravity-type retaining walls. An image processing system using a highspeed camera was set up to measure the dynamic deformation of the backfill soil. Earth pressures on the walls were measured with two-component load cells mounted on the wall centrelines. Displacement transducers and accelerometers were installed to measure the response of the retaining wall and the backfill. The backfill was air-dried Toyoura sand (D_{50} = 0.23 mm, specific gravity = 2.65, maximum and minimum void ratios of 0.977 and 0.609). The sand layers were prepared using a sand hopper to give an average relative density of 90%. Five models were tested. The subsoil and the predominant frequency of the input motion were varied between the tests. In Test 1 air-dried Toyoura sand was used as the subsoil, while in Tests 2–5 well compacted gravel was used. A steel plate, which was covered with sandpaper, was placed over the gravel subsoil in Tests 2-5 so that the failure mode was lateral sliding. The sliding friction was varied by using different grades of sandpaper. A strong motion that was recorded at the Kobe Marine Meteorological Observation Station during the 1995 Hyogo-ken Nambu earthquake was used as the base acceleration.

In two of the tests two distinct failure planes were observed. In Test 2 the first failure plane was at 56° to the horizontal and the second at 46°. In Test 3 similar planes developed at 58° and 50°. Development of the failure planes was not discussed in detail by Watanabe et al [9] and they did not give a clear indication of the seismic coefficient at which they developed. The critical acceleration coefficient to initiate sliding in Tests 2 and 3 was approximately 0.36. Sliding therefore commenced before high acceleration levels were reached. A Failure-Plane analysis using the peak and residual friction angles reported for the sand backfill of 51° and 43° indicated failure plane angles of 57° and 44° at acceleration coefficient levels of 0.24 and 0.47 respectively. The tests results therefore showed strain localization effects that were reasonably consistent with the Failure-Plane analysis method of Koseki et al [7]. The test results indicated that the force on the model walls could be calculated using the acceleration coefficient at which sliding commenced of approximately 0.36 (Tests 2, 3 & 4) and the peak backfill soil friction angle of 51°. The peak input base acceleration coefficient applied was approximately 0.95 and walls in Test 2 and 3 displaced 17.5 and 28 mm respectively. These displacement levels appeared consistent with predictions using Newmark Sliding Block theory (see below) but no detailed analyses were carried out.

GENERALISED MONONOBE-OKABE

Analysis Method

Shukla [10] presented a generalised analytical expression in explicit form for the pseudo-static earthquake active thrust from c–ϕ soil backfills acting on a rigid retaining wall. The expression is an extension of the M-O equation for cohesionless soil and as for the M-O analysis method assumes that sufficient outward movement of the wall occurs (translation or rotation) for active pressures to develop. The generalised analysis considers, inclination of the wall-soil interface, backfill slope angle, surcharge on the backfill, tension cracks, wall-backfill friction and adhesion, cohesion and angle of shearing resistance of the backfill, and both horizontal and vertical earthquake accelerations. An explicit analytical expression for the critical inclination of the failure plane within the soil backfill is also presented. Figure 22 shows the definition diagram for the generalised analysis.

Shukla [11] published the equivalent solution for passive pressure with the wall forced against the backfill and the horizontal inertia force acting on the soil wedge in the opposite direction to that shown in Figure 22.

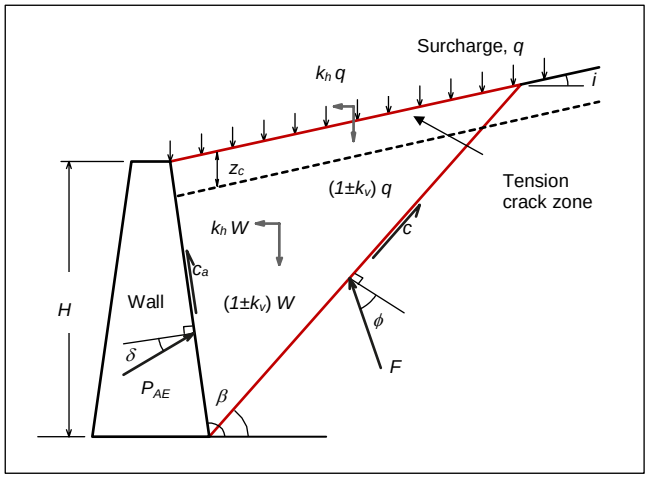

Figure 22: Forces acting on failure wedge for c-ϕ soil. (from Shukla [10]).

Active Pressure Force

The active earthquake pressure force P_{AE} on the back face of the wall from the failure wedge (including the gravity component) is given by:

$$P_{AE} = 0.5 K_{AE}\, \gamma H^2 \tag{10}$$

$$K_{AE} = (1 \pm k_v)\left[\frac{2q}{\gamma H} + \frac{\sin(\beta - i)}{\sin(\beta)}\right] K_{AE\gamma} \mp \frac{c}{\gamma H}\left[2 - \frac{z_c}{H}\right] K_{AEc} \tag{11}$$

$$K_{AE\gamma} = \frac{\sin(\beta - \alpha_c)\sin(\pm\theta \mp \emptyset + \alpha_c)}{\cos\theta\, sin\beta\, \sin(\alpha_c - i)\, \sin(\beta \pm \delta \pm \emptyset - \alpha_c)} \tag{12}$$

$$K_{AEc} = \frac{a_f \cos(\beta \pm \emptyset - \alpha_c) + \frac{\sin(\beta - i)cos\emptyset}{\sin(\alpha_c - i)}}{sin\beta\, \sin(\beta \pm \delta \pm \emptyset - \alpha_c)} \tag{13}$$

Where q is the vertical surcharge on the backfill surface, c the soil cohesion on the failure plane, c_a the adhesion on the wall-backfill interface, a_f the adhesion factor = c_a/c, z_c the tension crack depth, ϕ the peak soil friction angle, β the wall inclination (positive in an anticlockwise direction from the horizontal), δ

the friction angle on the wall-soil interface, i the soil backslope angle (from horizontal), α_c the critical failure plane angle and θ the seismic inertia angle given by:

$$\theta = tan^{-1}\left[\frac{k_h}{1 \pm k_v}\right] \quad (14)$$

Where k_h is the horizontal acceleration coefficient and k_v is the vertical acceleration coefficient.

Equations 10 to 14 can be used for the passive pressure case by applying the lower of the signs where both + and – signs are indicated. In the passive case z_c is assumed to be zero.

The angle parameters and the forces acting on the failure wedge in the backfill are shown in Figure 22.

Based on Rankine's analysis the tension crack depth can be taken as (Terzaghi et al, [12]):

$$z_c = \frac{2c}{\gamma} tan\left(\frac{\pi}{4} + \frac{\phi}{2}\right) \quad (15)$$

Equations 12 and 13 for $K_{AE\gamma}$ and K_{AEc} are in expressed in terms of the critical failure plane angle α_c. Shukla, 2015 gives closed form expressions for α_c but they are too complicated to present here. The critical angle can be determined by iteration to find the maximum value of K_{AE} (Equation 11). The Excel Solver add-in is a convenient method of undertaking this iteration directly and is a more straightforward method for calculating α_c than evaluating the closed form equations.

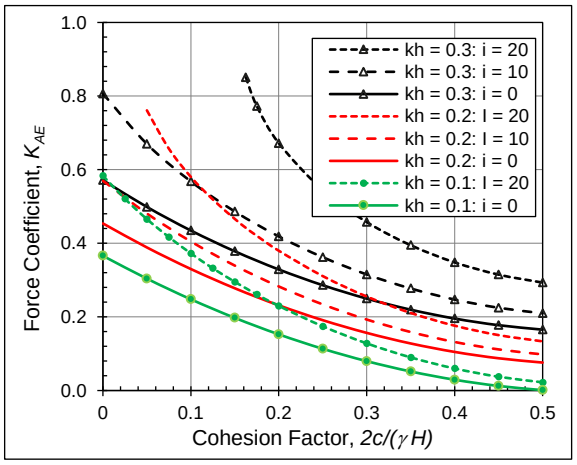

Figure 23: Force coefficient for $\phi = 30^o$.

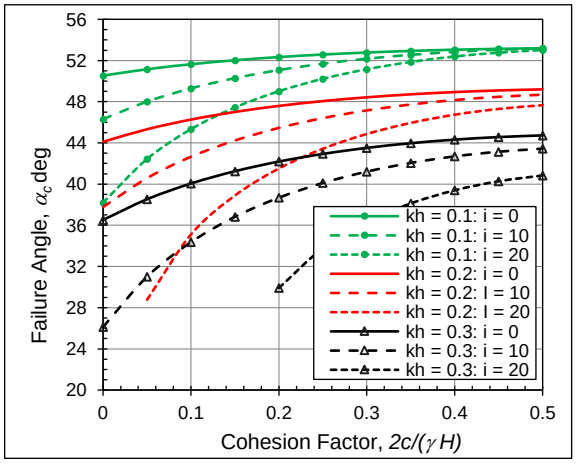

Figure 24: Failure plane angle for $\phi = 30^o$.

K_{AE} and α_c versus the cohesion factor $2c/\gamma H$ are plotted for a backfill with $\phi = 30°$ in Figures 23 and 24 respectively. Similar plots for a backfill friction angle of 35° are shown in Figures 25 and 26 respectively. Curves are shown for k_h values of 0.1, 0.2 and 0.3 and for each k_h value a backfill surface inclination curve is shown for i values of 0°, 10° and 20°. To calculate the results shown in Figures 23 to 26 it was assumed that z_c was as given by Equation 15, $\beta = 90^o$, $\delta = 2/3\phi$, $a_f = 0.5$ and $k_v = q = 0$. The force on the wall P_{AE} is calculated from K_{AE} using Equation 10 and is orientated at an angle δ to the normal to the wall as shown in Figure 22. Figures 23 and 25 show that small amounts of cohesion reduce the K_{AE} values significantly.

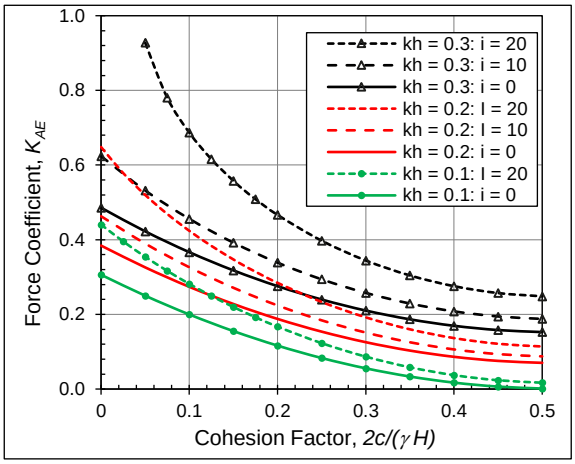

Figure 25: Force coefficient for $\phi = 35^o$.

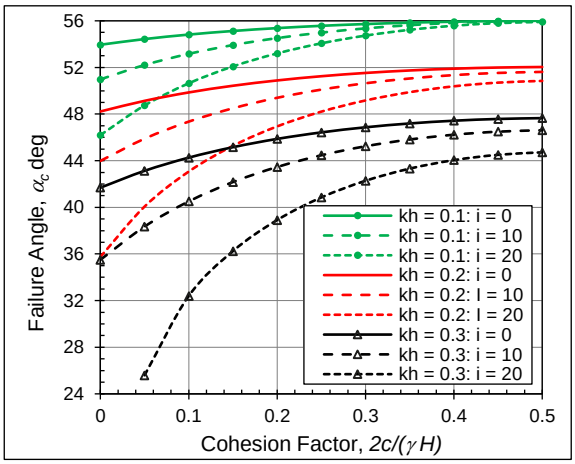

Figure 26: Failure plane angle for $\phi = 35^o$.

Failure Plane Location

It is important to estimate the failure plane angle for the backfill soil and consider the influence of the surrounding soil outside the limits of the backfill zone. When the failure plane angle is predetermined by the boundary between the backfill and a surrounding soil with significantly greater shear strength than the backfill, K_{AE} can be calculated using the predetermined angle in Equations 12 and 13 rather than α_c. This situation may arise where the soil (or rock) outside the backfill zone has significant cohesion.

A cantilever wall example where the design should be based on the interface angle between the backfill and residual soil is shown in Figure 27. The backfill was assumed to be cohesionless with a friction angle of $\phi = 30^o$ and the residual soil assumed to have the same friction angle but with cohesion of 10 kPa. Both soils had a unit weight of 20 kN/m^3 and the design earthquake acceleration coefficient was assumed to be 0.3. The residual soil was excavated on a 60° angle for the wall construction.

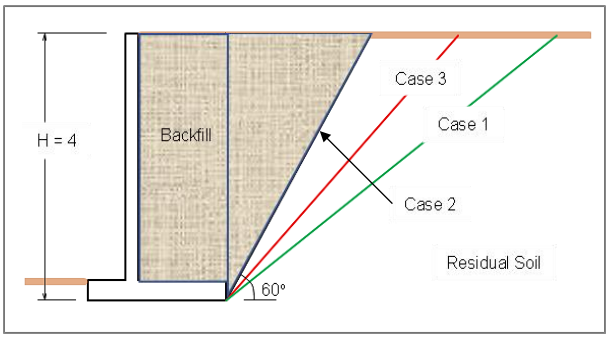

Figure 27: Failure planes for cantilever wall example.

The wall height was taken as 4 m and the friction angle on the virtual backface of the wall was assumed to be 20°. Force coefficients, K_{AE} , for the three potential failure planes shown in Figure 27 are listed in Table 4. For the Case 1 failure plane, the force coefficient was calculated using the M-O equations and assuming no cohesion in the residual soil. For Case 2 the failure plane was assumed to be on the interface between the backfill and the residual soil and for this case the force coefficient can be calculated using either the M-O or Shukla equations (Equations 10 to 13) with the failure angle set to 60°. For Case 3 the failure was assumed to be in the residual soil which was assumed to have 10 kPa cohesion (cohesion factor of 0.25) and no tension crack or wall adhesion. The Shukla equations were used for this case.

The force coefficients shown in Table 4 for Cases 1 and 3 demonstrate how a small amount of cohesion reduces the force coefficient by more than a factor of two (approximate solutions for the force coefficient and failure plane can be obtained from Figures 23 and 24). For this example, the design should be based on Case 2 with the force coefficient reduced by 21% from the value that would be obtained using M-O and assuming no cohesion in the residual soil.

Table 4: Force coefficients for cantilever wall example.

Analysis Case	Cohesion in Residual Soil	Failure Plane Angle	K_{AE} ($P_{AE} = 0.5\ K_{AE}\gamma H^2$)
1	0	37°	0.57
2	-	60° (interface)	0.45
3	10 kPa	47°	0.24

OUTWARD DISPLACEMENT

For high earthquake acceleration coefficients and walls with steep backfill slopes it will often be advantageous to design for permanent displacements arising from sliding and rotation of the wall, soil foundation deformation or ductility in the wall structure. The design can then be based on the critical acceleration to initiate permanent displacement rather than the PGA.

Displacement Theory

The outward movement of walls resulting from sliding, foundation bearing failures, or a ductile failure in the wall structure can be estimated using the Newmark Sliding Block theory [13]. The soil mass is assumed to be a rigid block that fails in a rigid-plastic manner when the ground acceleration exceeds the critical or yield acceleration of the slope. Once sliding commences, it is assumed that the rigid mass continues to slide under the actions of the inertia force from the ground acceleration pulse and a constant resisting force. When the acceleration pulse diminishes in magnitude or reverses in direction, the relative velocity between the sliding block and the supporting ground or base eventually reduces to zero and the movement relative to the base ceases. Successive displacements take place each time the ground acceleration exceeds the critical value. Newmark considered the case of both symmetrical and unsymmetrical sliding. In the second case the sliding movement was assumed to accumulate in only one direction. This case is appropriate for downslope movements of slope failures or retaining walls where movement in one direction is resisted by gravity forces in the case of a slope failure, or passive resistance in the case of a wall leading to the critical acceleration in one direction being much higher than in the other.

Outward movement can be estimated using the Jibson [14] correlation equation. This equation was derived by statistical analysis of the displacements calculated from numerical sliding block computations using 2,270 strong motion acceleration records. The Jibson equation for the mean permanent outward displacement, d expressed in centimetres is given by:

$$\log(d) = -0.271 + log\left[\left(1 - \frac{a_c}{a_{max}}\right)^{2.335}\left(\frac{a_c}{a_{max}}\right)^{-1.478}\right] + 0.424M_w \quad (16)$$

Where a_c is the critical acceleration to initiate sliding failure, a_{max} is the PGA in the acceleration record, and M_w the earthquake moment magnitude. The displacement is normally distributed with a standard deviation of 0.454. Evaluation of Equation 16 requires the calculation of the a_c /a_{max} ratio, selection of an appropriate earthquake magnitude and deciding on an appropriate level for the probability of exceedance of the calculated displacement using the standard deviation. Similar regression equations have been developed by Ambraseys and Menu [15]; Ambraseys and Srbulov [16]; Anderson et al [17], and Bray et al [18].

A displacement versus a_c /a_{max} curve from the evaluation of Equation 16 for M_w = 7.0 and a 16% probability of exceedance is compared in Figure 28 with the other displacement correlation equations mentioned previously. For a_c /a_{max} ratios of between 0.3 to 0.7 displacement estimates vary by a factor of about two. Some of the variation results from different factors used in the equations which makes direct comparison approximate. Jibson's study was probably the most comprehensive and his equation is the preferred correlation. For design an average value of the curves could be adopted.

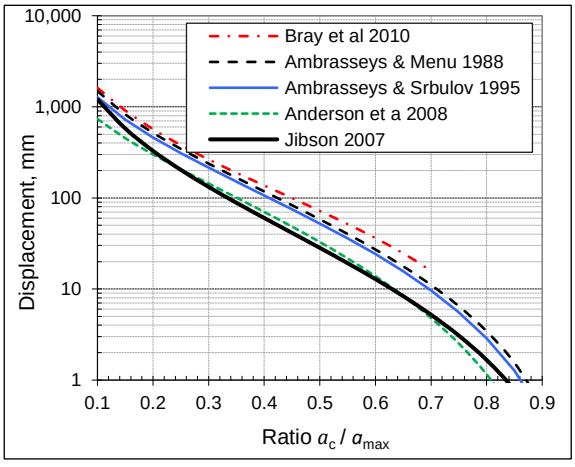

Figure 28. Displacements from correlation equations.

Figure 28 shows that for a critical acceleration of one-half of the PGA the permanent outward movement of the sliding mass in a M_w 7.0 earthquake is likely to be in the range of 30 to 70 mm (16% probability of exceedance). Many wall structures would not be seriously damaged by movements of this order.

Increasing M_w to 7.5 increases the Jibson displacement from 28 mm to 46 mm (64% increase) and the Ambraseys and Srbulov displacement by a similar percentage increase.

Some rotation of a wall structure may occur when the wall slides outward and it is therefore likely that the displacements at the top of the wall could be up to 50% higher than estimated from the rigid siding block assumption.

Model Tests

Outward displacements were measured in model wall tests carried out by Lai [19] (Lai and Berrill [20]; Wood and Elms [21]) to investigate the sliding block method for predicting the critical acceleration and the outward displacement of gravity type retaining walls. The tests were carried out using a 2.4 m long, 510 mm wide glass-sided rectangular tank mounted on an electro-hydraulic shaking table. The model was 300 mm high, backfilled to 250 mm above its base and rested on a 100 mm depth of soil below the base. Provision was made to add mass to the model base by bolting on steel plates. The low centre of gravity ensured translational rather than rotational failure.

Bending moment and vertical and horizontal shear forces on the rear face of the model wall were measured with strain gauges on the wall stem. Displacements of the top of the wall relative to the tank were measured with two displacement transducers and two accelerometers were used to record the tank and wall base accelerations. A uniform fine to medium sand, with an angle of internal friction reported to be about 30° was used in the tests.

Tests were carried out using both a 5 Hz sinusoidal excitation and scaled accelerograms recorded during the 1940 El Centro and 1966 Parkfield earthquakes. Several series of tests were carried out using different wall weights. There was good similarity between the measured and predicted displacement results based on the Newmark theory but the measured displacements were less than predicted. Some of the differences were caused by a lowering of the backfill with increasing displacement and changes in the base friction during the shaking. The base friction may have been greater than assumed in the analyses. There was good agreement between the measured values and theoretical M-O predictions of the critical accelerations to initiate sliding using a base friction angle of about 25°. The conclusion from the work was that the sliding block theoretical model predicted the observed sliding behaviour of the model wall remarkably well.

SUBMERGED BACKFILL SOIL

Matsuzawa et al [22] developed a method for calculating lateral earthquake pressures against a rigid wall from soil and water when the backfill soil is submerged. The method is based on the M-O analysis procedure for unsaturated backfill soil.

Highly Permeable Backfill

For highly permeable soils Matsuzawa et al [22] assumed that the pore water can move freely in the voids without restriction from the soil particles. The vertical body force during the earthquake can be calculated by subtracting the dynamic buoyancy force acting on the solid particles from the total dynamic force. Therefore, the apparent seismic inertia angle θ' can be calculated by:

$$tan\theta' = \frac{F_H}{F_V} = \left(\frac{G_s}{G_s - 1}\right)\left(\frac{k_h}{1 \pm k_v}\right) = \frac{G_s}{G_s - 1} tan\theta \qquad (17)$$

Where G_s is the specific gravity of the soil particles. For most soils G_s is approximately 2.6 so the effective seismic coefficient is about 1.6 times the true seismic coefficient for an unsaturated backfill soil.

For a highly permeable soil a dynamic water pressure needs to be added to the pressure from the soil particles. Westergaard [23] proposed the following approximate solution for the water pressure force on a vertical wall with a semi-infinite long water reservoir:

$$P_{wd} = \frac{7}{12} k_h \gamma_w H_w^2 \qquad (18)$$

Where γ_w is the unit weight of water having a height of H_w above the wall base. The water pressure force acts at a height 0.4 H above the base of the wall. The water flow will usually be restricted by the soil particles and boundaries so Equation 18 will give a conservative estimate of the water force.

Low Permeability Backfill

For low permeability backfills Matsuzawa et al [22] assumed that the solid portion and the pore water portion of the soil element behave as a unit. Therefore, the total unit weight of the soil is subjected to the horizontal acceleration and thus the horizontal inertia body force, F_H is equal to $\gamma_{sat} k_h$. The apparent inertia angle of the seismic coefficient becomes:

$$tan\theta'' = \frac{F_H}{F_V} = \frac{\gamma_{sat}}{\gamma_{sub}}\left(\frac{k_h}{1 \pm k_v}\right) = \frac{\gamma_{sat}}{\gamma_{sat} - \gamma_w}\left(\frac{k_h}{1 \pm k_v}\right) tan\theta \qquad (19)$$

Where γ_{sat} and γ_{sub} are the saturated and submerged unit weight of the soil respectively.

The saturated unit weight of soil is approximately two times the unit weight of water giving an effective horizontal seismic coefficient of approximately two times the value for unsaturated soil.

Since the static lateral pressure is contributed only by the effective vertical stress in both the high and low permeability soil cases the soil submerged unit weight, γ_{sub} should be used in the M-O equation used to calculate the force from the K_{AE} pressure coefficient (Equations 5 and 10). The submerged unit weight is given by:

$$\gamma_{sub} = \gamma_{sat} - \gamma_w \qquad (20)$$

Forces from High and Low Permeability Backfill

Figure 29 shows a comparison of the dimensionless horizontal force, $P_{AEd} = P_{AE}/(0.5\gamma_{bulk} H^2)$ acting on a rigid wall for an unsaturated backfill soil, with saturated backfill having both high and low permeability over the range of k_h values used in design. The bulk unit weight of the soil, γ_{bulk} was assumed to be 18 kN/m^3, the saturated unit weight 19.5 kN/m^3 and the soil specific gravity 2.65. The earthquake force is shown for soil friction angles, ϕ of 35° and 30° (cohesionless soil) with the friction angle on the wall-soil interface taken as 2/3ϕ.

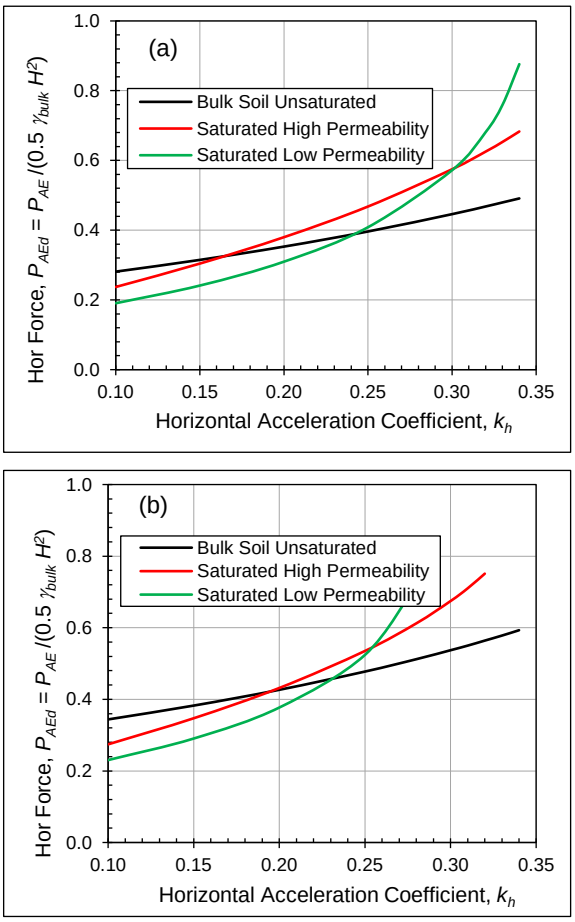

Figure 29: Earthquake force from unsaturated and saturated soil (a) $\phi = 35^o$: (b) $\phi = 30^o$.

Over the k_h range of interest for low walls of 0.15 to 0.25 there is only a small difference between the force from unsaturated (based on bulk density) and the force from saturated high permeability soil (including the dynamic water force). Matsuzawa et al [22] developed a generalised apparent inertia angle to cover a wide range of backfill types with intermediate permeabilities but for wall design Figure 29 shows that for k_h values less than 0.3 for $\phi = 35^o$ and less than 0.25 for $\phi = 30^o$ assuming a high permeability soil gives a moderately conservative result for all permeabilities.

Hydrostatic and hydrodynamic (if any) forces on the wall must be added to the soil force from the M-O analysis.

Partially Submerged Backfill

For the case when the water level is below the top of the wall Kramer [24] suggested that the earthquake soil force on the wall could be computed using an average unit weight based on the relative volumes of soil within the active wedge that are above and below the phreatic surface (γ_{bulk} above water level and γ_{sub} below). The geometry for this partially saturated backfill case is shown in Figure 30. Kramer did not make any suggestions on what inertia angle should be used for this partially submerged case. The writer considers that a better approach than using the average unit weight in the failure active wedge would be to calculate the M-O force for both cases of a fully saturated and unsaturated backfill and average these two forces based on the relative volume of soil within the active wedge.

The average M-O force P_{AEav} is then given by:

$$P_{AEav} = P_{AEsat}\lambda^2 + P_{AEbulk}(1 - \lambda^2) \qquad (21)$$

Where P_{AEsat} and P_{AEbulk} are the M-O forces from assuming the backfill is completely saturated and completely unsaturated respectively. λ is the fraction of the total height of saturated backfill measured from the base of the wall (Figure 30). If λ is less than about 0.2 the M-O force can be computed ignoring the water in the backfill but the static water pressure should still be included in the computation of the force on the wall.

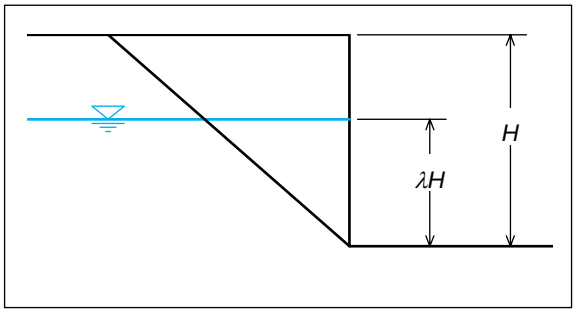

Figure 30: Geometry and notation for partially saturated.

REDUCTION FROM WAVE SCATTERING

Anderson et al [17] carried out studies on seismic wave incoherence or scattering to evaluate the relationship between the average ground acceleration behind retaining walls (and within slopes) to the input acceleration at a transmitting boundary beneath the wall, as a function of height of the wall. Wave propagation analyses were carried out using elastic two-dimensional FEA models of both retaining walls (and slopes). The model used for these analyses had the following characteristics:

- The soil was assumed to compacted fill with a shear wave velocity of 240 m/sec.
- The base transmitting boundary was set at a distance of approximately 40 m below the base of the wall.
- The half-space beneath the transmitting boundary was assigned a shear wave velocity of 240 m/sec, identical to the soil mesh above the transmitting boundary. Using a uniform soil property meant that the ground shaking would be the intended free-field motion at the ground surface.
- A free boundary at the wall face was assumed.

Figure 31 shows one of the wave scattering analysis model used for the retaining wall analysis. Four models with wall heights of 6.1 m, 12.2 m, 24.4 m and 45.7 m were investigated. Three failure blocks delineated by the failure planes shown in Figure 31 were investigated. Input acceleration time histories were scaled to three spectral shapes with three time histories for each spectral shape.

The input motion spectral shapes were named Upper Bound (UB), Mid and Lower Bound (LB). The ratio of the 1-second acceleration spectral ordinate to the zero-period ordinate were approximately 1.7, 1.2 and 0.4 for the UB, Mid and LB spectra respectively. The Mid spectral shape corresponded approximately to the Soil type C spectrum (1-second spectral ordinate ratio of 1.2) given in NZS 1170.5 [25]. The UB spectrum corresponded approximately to the Soil type D NZS1170.5 spectrum (1-second spectral ratio of 1.9). The analysis results for the Mid spectrum were scaled to approximately represent the results expected for Soil types A & B of NZS 1170.5 using the 1-sesond spectral ratios (1.2 for the Mid spectrum and 0.95 for Soil type A & B spectrum).

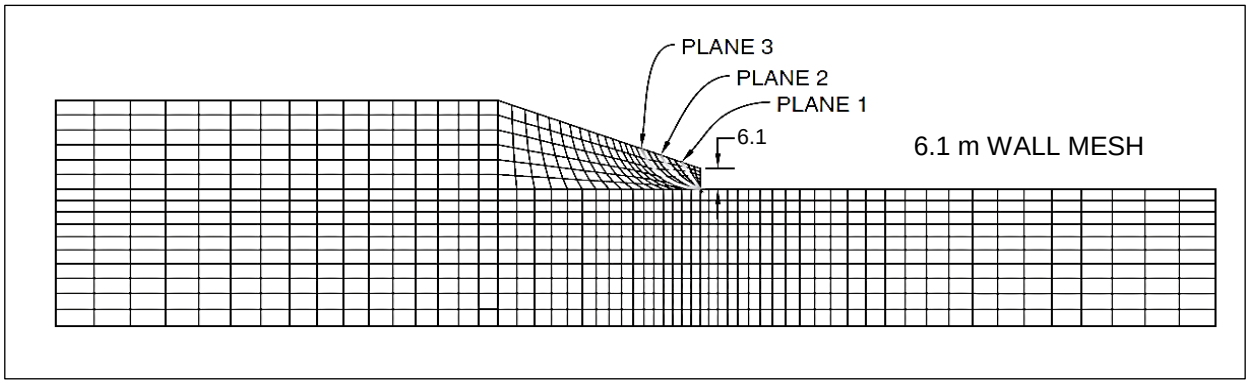

Figure 31: Wave scattering model from Anderson et al [17].

The results from the study were presented as a scaling factor, α defined as the ratio of the average peak acceleration response in the wall failure block to the PGA of the input motion.

Results from the three time histories matched to each response spectrum were averaged. The variation in the scaling factor was not very significant between the three failure blocks evaluated for each scaling factor for each height and these results were also averaged to give a single scaling factor for each wall height.

The investigation showed that the wave scattering scaling factor systematically decreased for increasing wall height and lowering of the spectral shape at long periods. Results for the average α factors categorized by wall height and the spectral shapes (using the NZS1170.5 soil type notation) are summarized in Figure 32.

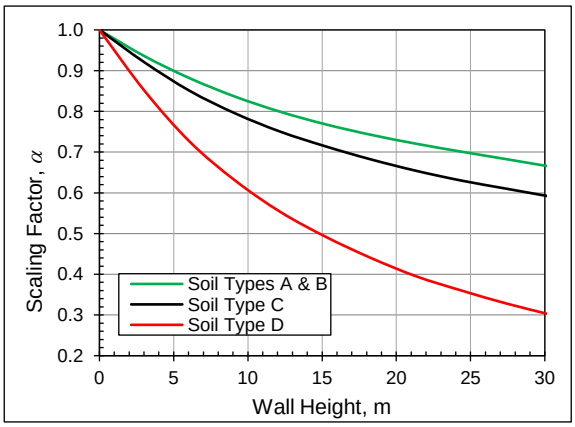

Figure 32: Wall height scaling factor [17].

Figure 32 shows that for wall heights less than 5 m the reduction in the input PGA by wave scattering is not very large. For a 5 m wall height the α factor is 0.9, 0.87, 0.77 for soil types, A & B, C and D respectively.

A pseudo-static earthquake load analysis treats the seismic coefficient as a constant horizontal static force applied to the backfill soil mass. However, Anderson et al point out that the peak acceleration load occurs for a very short time with the average seismic force typically ranging from 30 to 70 percent of the peak depending on the characteristics of the specific earthquake event. They suggest that a further reduction in the pseudo-static force reflecting the overall average cyclic loading might be justified where a structural system is designed for some degree of ductile yielding. (As indicated above, designing for a static force less than the inertia force from the PGA in the input motion can be used when the wall is designed to move outwards.)

SLIDING RESISTANCE AND PASSIVE PRESSURES

Cohesionless Foundation Soil

The sliding resistance of cantilever and gravity walls is usually taken as the sum of the friction force on the base of the footing and the passive resistance on the effective toe depth of the wall. Figure 33 shows the failure slip lines calculated using LS: Geo [4] for a 2.5 m high cantilever wall subjected to gravity, live load of 4 kPa and horizontal earthquake loads. Both the backfill and foundation soil were assumed to be cohesionless with a friction angle of 30°.

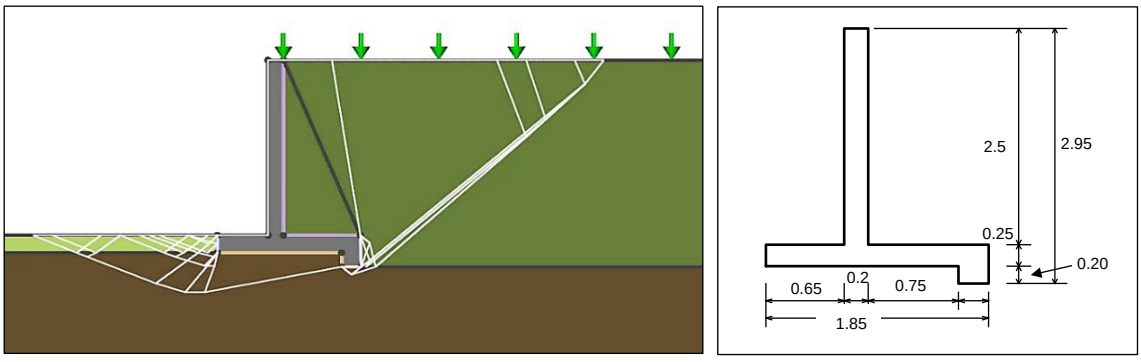

Figure 33: Failure slip-lines for cantilever wall.

All soil-wall interfaces were set to a friction coefficient of $0.5\tan\phi = 0.29$. The critical acceleration to initiate sliding displacement was 0.23 g. The slip lines indicate that the 0.2 m deep key at the rear of the footing has a significant influence on sliding resistance and suggest that the depth to be used in estimating the passive resistance should be taken as at least the sum of the footing and key depth. The key also initiates failure through the soil rather than on the interface of the soil with the footing base.

Numerical results for the passive resistance of a cohesionless soil-wall interface under earthquake loading have been presented by Choudhury [26]; Kumar [27]; Morrison and Ebeling [28]; Mylonakis et al [29]; Soubra [30], and Subba Rao & Choudhury [31]. The M-O equation can be used to calculate the passive resistance (with sign changes from the active case) but significantly overestimates the resistance for friction angles greater than 30° and when there is significant soil-wall interface friction.

Results from Soubra [30] for the earthquake force passive pressure coefficient on a vertical wall with a horizontal ground surface are shown in Figure 34 for soil friction ϕ angles of 30°, 35° and 40°.

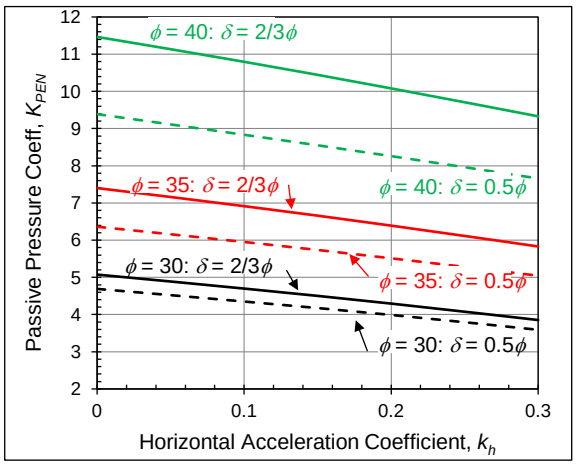

Figure 34: Passive pressure coefficient for cohesionless soil [30].

Pressure coefficients for two soil-wall interface friction values of 0.5ϕ and $2/3\phi$ are shown for each of the soil friction values. The passive pressure coefficient K_{PEN} is for the force component normal to the wall. Soubra used a translational multiblock failure mechanism which is essentially a generalisation of the single block used in the M-O analysis method. A comparison of the Soubra [30] pressure coefficients with the results from the other researchers mentioned above showed good agreement.

Cohesive Foundation Soil

For purely cohesive soils the Shukla [11] generalised analytical expressions given in Equations 10 to 13 above can be used to estimate the passive pressure acting on a soil-wall interface. For a vertical wall face, a horizontal ground surface and assuming a plane failure surface these equations can be simplified to give the dimensionless passive pressure force normal to the wall as:

$$P_{PED} = \frac{P_{PE}}{0.5\gamma H^2} = (cosec(\alpha_c)sec(\alpha_c))\frac{2c}{\gamma H} + (1 - k_h\cot(\alpha_c)) \qquad (22)$$

The critical failure plane angle from the horizontal is given by:

$$\alpha_c = arctan\sqrt{\frac{1-\frac{k_h\gamma H}{2c}}{1+a_f}} \qquad (23)$$

A plot of the dimensionless passive pressure force P_{PED} versus the cohesion factor, $2c/(\gamma H)$ is shown in Figure 35 for k_h values of 0, 0.2 and 0.4. The a_f value (adhesion on the soil-wall interface) was taken as 0.5. Except for low cohesion factors the pressure force varies almost linearly with this ratio.

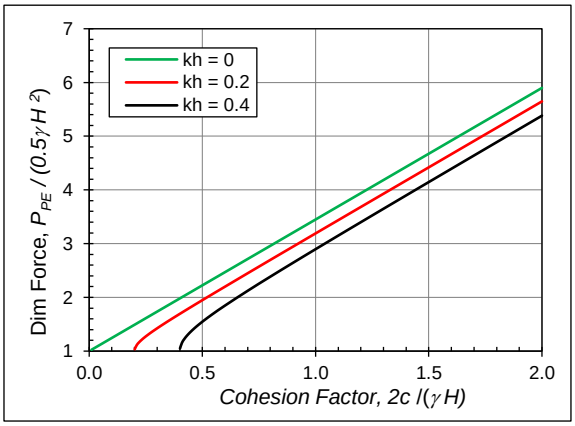

Figure 35: Passive pressure force for cohesive soil.

c-φ Foundation Soils

For soils with both cohesion and friction the solutions of Soubra [30] and Shukla [11] can be applied but both have limitations. For friction angles greater than 30° and high soil-wall interface friction the plane failure surface assumption of Shukla results in an overestimation of the passive force. Soubra's numerical results are only tabulated for friction angles greater than 15° but provided the friction angle is greater than this value these results give values suitable for design. An acceptable approach for design when the backfill friction angle is greater than 30° would be to add the friction component shown in Figure 34 to the cohesion component shown in Figure 35. For friction angles less than 30° the Shukla equations can be used and should give acceptable force predictions although possibly too high by a small amount. (Reference can be made to the Soubra [30] results for ϕ down to 15°).

Location of Shear Key

The location of the shear key has a major influence on the sliding resistance under both gravity and earthquake load cases for a cohesionless foundation soil but has little influence for an undrained cohesive foundation soil. An analysis of the cantilever wall shown in Figure 33 using LS: Geo and the cohesionless soil described above for this wall with the key located at the front of the footing, under the stem and at the rear of the footing gave critical accelerations to initiate sliding of 0.07g, 0.15 g and 0.23 g respectively indicating significant benefits in locating the key at the rear of the footing.

Comparison with Experimental Results

To investigate bending moments in the stem of cantilever walls and their sliding resistance, analyses using the cantilever wall model shown in Figure 36 were undertaken as part of the present study. The dimensions were chosen to model the centrifuge experimental study reported by Mikola and Sitar [5] of a cantilever wall in cohesionless soil. Their experimental studies of cantilever wall model were carried out in conjunction with the U-wall model described above. The centrifuge model was a 1/36 scale model of a protype wall and was subjected to a 36 g acceleration in the centrifuge.

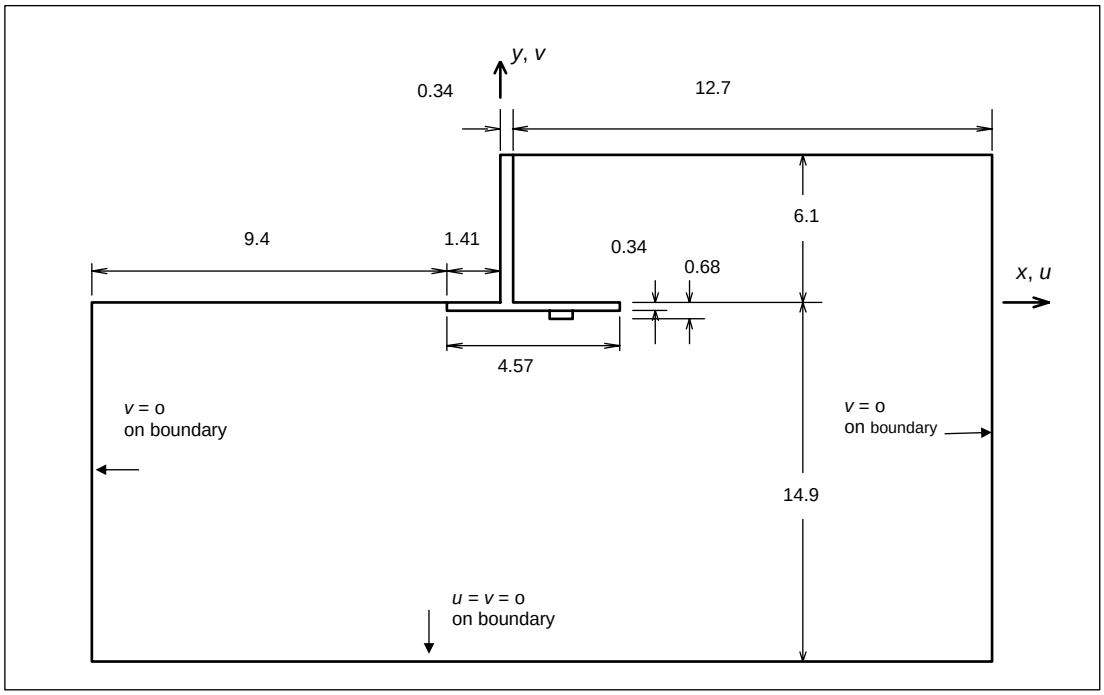

Figure 36: Cantilever wall model from [5].

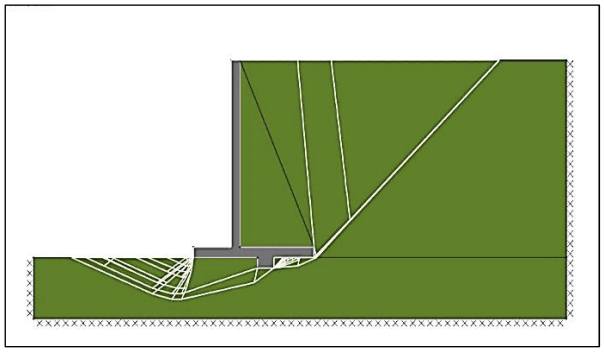

Figure 37: LS: Geo slip lines at critical acceleration of 0.26g.

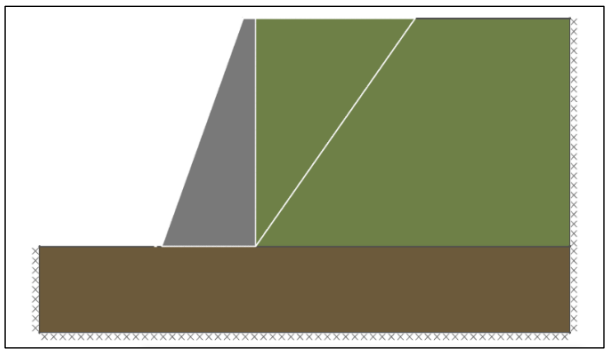

Figure 38: LS: Geo failure at critical acceleration of 0.34g.

Dimensions shown in Figure 36 are the prototype dimensions with the wall stem having a height of 6.12 m. As was the case for the U-wall, the cantilever model wall was constructed of aluminium alloy and the properties of this material were used in the analyses of the prototype. The soil used in the model study was Nevada sand which is a fine uniformly graded angular sand. Material properties for the sand (both model and prototype) are summarised in Table 1. Both the cantilever wall stem and foundation footing were 0.34 m thick resulting in the cantilever wall being considerably more flexible that the U-wall.

In the present study elastic FEA and LS: Geo analyses were carried out. Earthquake loading was applied as a uniform horizontal body force acting within the soil. Analyses were carried out for the same uniform acceleration acting on the wall and for the case when the inertia force on the wall was zero. This later case was achieved in the analysis by assuming zero for the unit weight of the wall.

Elastic FEA analyses were undertaken for soil Young's moduli of both 100 MPa and 50 MPa. Wall stem stiffness parameters (d_w) were 37.5 and 18.8 for the 100 MPa Young's modulus and reduced modulus values respectively so the wall stem acted as a flexible wall under earthquake loads.

In the LS: Geo analysis the interfaces between the soil and wall were assumed to have a friction coefficient of 0.5 x tan (soil friction angle) = 0.36 with all the soil assumed to be cohesionless with a friction angle of 36^o. This analysis gave a critical acceleration of 0.26 g. Failure slip lines that developed in the soil are shown in Figure 37.

In the experimental centrifuge model of Mikola and Sitar [5] it appeared the soil level in front of the wall was at the base of the foundation slab. If the soil level was at the top of the base slab with passive resistance against the wall toe the critical acceleration would increase to 0.31 g (19% increase).

For the case with the soil in front of the wall at the underside level of the foundation slab the passive resistance against the 0.34 m deep shear key is a very significant component of resistance being about 38% of the total sliding resistance.

Although Mikola and Sitar did state specifically at what level sliding of the wall occurred their plot of deflections shows significant "rigid body" displacements at accelerations greater than 0.25 g (see Figure 41 below) indicating reasonable agreement with the LS: Geo analysis.

As mentioned above, failure plane development was monitored by Watanabe et al [9] in a series of shaking table tests on 530 mm high model gravity-type retaining walls (one-g gravity). Four of the five model walls were on a rigid foundation base so were much simpler models than the wall in the Mikola and Sitar tests. Details of the wall and soil are summarised in Table 5.

Table 5: Material properties for Watanabe et al wall model.

Soil Properties (Backfill & Foundation)			
Unit weight	γ	16 kN/m^3	Relative density = 90%
Peak soil friction angle	ϕ	51^o	Used in M-O analysis
Wall-backfill interface friction	δ	25.5^o	(Watanabe et al assumed 0.75ϕ)
Wall foundation-interface friction	ϕ_b	32^o	Measured values 31^o to 34^o
Wall Properties			
Unit weight	γ_w	22.7kN/m^3	Weight of 938 N & width of 0.6 m
Wall height	H	530 mm	
Top thickness	t_w	30 mm	
Base thickness	B_w	230 mm	

The test results showed wall sliding commencing at an acceleration coefficient of approximately 0.36 (Tests 2, 3 & 4). A LS: Geo analysis using the properties summarised in Table 5 indicated that sliding would commence at an acceleration coefficient of 0.34. A simple M-O hand analysis indicated a slightly higher limiting acceleration coefficient of 0.4. The M-O failure angle from the horizontal was 51^o and this was a little lower than the angle of 53^o estimated from the slip line geometry shown by the LS: Geo analysis. Figure 38 shows the wall shape and the failure slip line in the backfill from this analysis.

As mentioned above, one-g model tests carried out by Lai [19] showed good agreement between measured and the M-O critical accelerations. Additional one-g model wall tests were carried out by Jacobsen [32] and Aitken [33] using a similar model wall to Lai. Jacobsen observed that the acceleration of the wall increased above the critical level required to initiate sliding until the wall acceleration exceeded the shaking table acceleration.

Aitken [33] found that the initial density of the sand used in his tests changed with outward movement of the wall. In-situ soil properties were measured by pulling the wall with a load cell and observing the failure force and the angle of the resulting static failure wedge. The wall was also pulled with no backfill behind the wall. These tests enabled estimates to be made of the backfill friction angle and the friction angles against both the backface and base of the wall. Failure development was examined in the tests by using time-lapse photography and single pulses rather than continuous shaking. Initially the acceleration to initiate sliding was very high with no clear failure surface developing but a zone of shear distortion growing from the base of the wall. The initial acceleration response of the wall did not have a plateau and equilibrium analysis implied an angle of internal friction tending towards the maximum attainable by the sand in its densest possible state (far higher than the placement density). On the application of subsequent pulses, a failure surface grew from the foot. Following full development of the failure surface the wall failed with an acceleration plateau corresponding to the M-O sliding-block assumption and with a value close to that predicted by the maintainable (large shear displacement) angle of internal friction.

Results from the Lai, Jacobsen, and Aitken tests are summarised in Wood and Elms [21].

Bending Moment Calculation for Cantilever Stems

For cantilever walls with significant heel widths, it is unclear how the soil above the heel influences the pressures on the stem. In conventional analyses it is usual to calculate the M-O pressures on a virtual back plane at the rear of the foundation slab heel. The weight of the soil on the heel is usually large and this will generate significant inertia force pressure on the stem in addition to the M-O pressures on the virtual back plane.

Pressure forces acting on the cantilever stem of the Mikola and Sitar wall shown in Figure 36 were calculated using LS: Geo. The horizontal force per unit height acting on the back plane calculated by a M-O analysis (including gravity) and the difference between this force and the forces form the LS: Geo analysis on the stem are shown in Figure 39. Also shown is the force per unit height from the inertia load on the weight of soil on the heel (between the back of the stem and the virtual back plane) assuming that this force produces a triangular pressure distribution. There is approximate agreement between this force from soil on the heel and the difference between the M-O pressure force and the LS: Geo pressure force with the difference between the two being greater near the top of the wall. The LS: Geo analysis assumed rigid wall behaviour and therefore does not take into account the flexibility of the cantilever. Considering this approximation, it would be satisfactory for design to add to the M-O pressures on the virtual backplane a heel inertia force with a triangular pressure distribution.

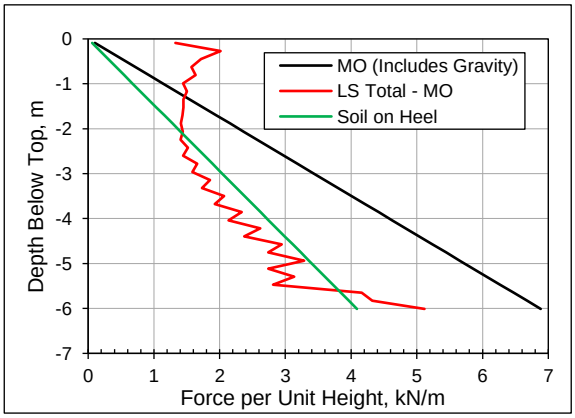

Figure 39: Pressure forces on cantilever wall stem.

For the Mikola and Sitar cantilever wall analysis the total LS: Geo moment at the base of the stem was 423 kN m (k_h = 0.26). The moment from the M-O analysis (including gravity) was 242 kN m and from the heel soil assuming a triangular pressure distribution 143 kN m giving a total moment of 385 kN m or about 9% less than the LS: Geo moment.

Bending Moment Comparison with Experimental Results.

As was the case of the U-wall the Mikola and Sitar report [5] contained plots of the total dynamic bending moments in the cantilever wall stems estimated from the stem strain gauge readings. To obtain the dynamic component they subtracted the static component assuming active pressures. Their main wall force and moment results are shown with the inertia effects of the wall removed from the dynamic component. As was the case for the U-wall the pressure modification from the wall inertia does not appear to have been considered in the results presented by Mikola and Sitar with their reduction to the total moments from wall inertia effects being much greater than indicated by the elastic FEA carried out in the present study.

Because of the uncertainty in the wall inertia moments the comparison between the elastic analyses and centrifuge

experimental results was only made in detail with the results with the wall inertia included. Figures 40 and 41 show comparisons between the elastic and experimental results for the stem base bending moment and the stem top deflection ratio respectively. The FEA results are the average of the values calculated for the smooth and bonded wall stem/soil interface assumptions.

There is reasonable agreement between the stem base bending moments and elastic FEA results below PGAs of 0.34. Sliding commences at about this level and the behaviour at higher accelerations becomes more complex. At a PGA of about 0.3 g the bending moment from a M-O analysis is a factor of 1.75 greater than the elastic bending moment. In the M-O analysis no adjustment has been made for the inertia of the wall or the weight of soil on the wall heel so overall there is a large difference between the experimental results and a conventional M-O analysis.

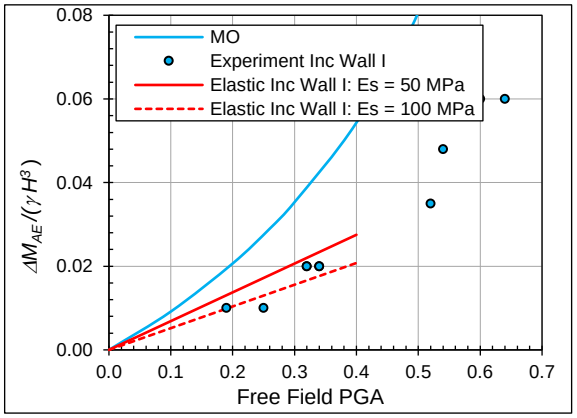

Figure 40: Moment at base of stem – earthquake component.

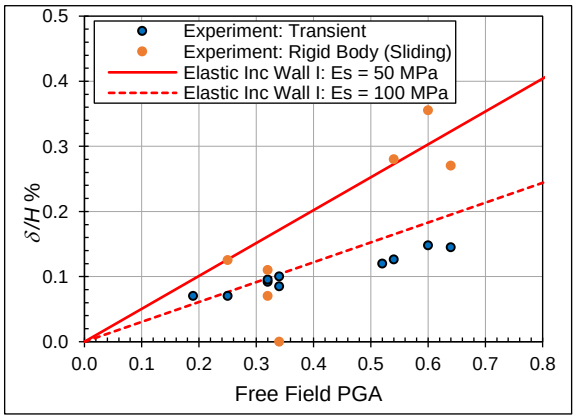

Figure 41: Deflection ratio for top of cantilever stem.

One major reason is that this particular cantilever wall is very flexible both in terms of the cantilever flexure and the base rotation. As mentioned above the flexure stiffness parameters (d_w) were 37.5 and 18.8 for the 100 MPa and 50 MPa Young's modulus values respectively. Corresponding values of the rotation parameter (d_θ) were 10.3 and 7.9 (average of bonded and smooth wall cases and with inertia of the wall included.) The rotation stiffness was increased significantly by rotation in the monolithic joint between the wall stem and foundation slab. In all the elastic FEA's the wall separated from the soil over the top ¼ to ½ of the cantilever stem (the amount varies with soil modulus wall/soil contact and wall inertia assumptions). This separation results in a large reduction in the stem bending moments. In low levels of shaking the model behaviour would be affected by this separation effect. At higher shaking levels the nonlinear soil response would reduce the separation and is one explanation for the experimental bending moment results increasing significantly at PGA's greater than 0.5 g. With wall sliding commencing at about 0.3 g this increase would otherwise be unexpected.

There is moderately good agreement between the FEA displacement ratio results based on a Young's modulus of 100 MPa and the experimental values indicating that deflections can be estimated by simplified analyses. The deflection ratio is less influenced by the wall separation effect than the stem bending moments. The combined experimental transient and rigid body (or sliding) displacements indicating that active pressures on the wall stem were likely at PGA's greater than about 0.35 g.

CONCLUSIONS

Implications for Design

The elastic flexibility of the wall and wall foundation, and the ability of the wall to move permanently by translation or rotation from inelastic action in the foundation or structure should be evaluated to determine whether the M-O method can be applied.

The experimental work investigated as part of the present study indicated that when applicable the M-O method gave moderately conservative predictions for the earthquake forces on free-standing walls. Arbitrary reductions to the PGA to predict the acceleration acting on the failure wedge are often made (for example see [34] and [35]). For major walls reductions in the design level PGA and estimates of outward displacements should be based on the following considerations.

- Where outward wall movement is acceptable, a reduction in the PGA should be based on the Jibson correlation equation for estimating permanent displacement.
- The average of best estimates of the peak and residual shear strengths should be used to calculate the critical acceleration rather than conservative residual values.
- Allowance should be made for the effects of cohesion in the backfill and residual soil. If the shear strength of the residual soil is significantly greater than the backfill the size of the failure wedge should be reduced by taking the failure surface as the interface between the backfill and residual soil.
- When estimating the critical acceleration to initiate a sliding failure the passive resistance of the shear key and foundation toe should be determined using best estimates of the effective depth and soil shear strength rather than conservative values.
- For high walls, a reduction in the failure wedge inertia force from wave scattering effects should be applied.
- Where the water height in the backfill is less than 0.2 times the wall height the M-O force can be computed ignoring the water in the backfill.

For stiff walls where the M-O method is not applicable an estimate of the design earthquake forces acting on the wall and the wall deflections can be made using the wall flexibility charts from [3] and reproduced above. Most wall structures have relatively simple geometries enabling elastic FEA models to be easily generated to enable the chart information to be extended for more complex foundation and boundary conditions. Static analyses will give moderately conservative predictions of the earthquake pressures. The method can be refined by using elastic dynamic modal analysis which can sometimes be more informative than static analyses. Although soil properties cannot be accurately represented by elastic assumptions, for many walls insufficient soils information will be available to justify more complex nonlinear static or dynamic FEA.

Other Conclusions

The refinements to the M-O method investigated in the present study are not difficult to evaluate. Charts presented in the paper provide a quick method of assessing whether a more detailed analysis is required.

For walls with simple geometry (usually the case) the LS: Geo software is easy to apply and can be used to investigate the influence of the wall geometric parameters on the critical acceleration to initiate permanent displacements in design applications where the M-O method is applicable. LS: Geo was used in the present study to estimate the pressures on the stem of a cantilever wall from earthquake inertia loads acting on the soil resting on the wall heel in addition to the M-O pressure on a virtual backface. It was found that the inertia force from the soil on the heel could be represented by a triangular pressure distribution on the stem.

ACKNOWLEDGEMENTS

Some of the material in his paper was prepared as part of the author's review involvement with the NZ Geotechnical Society's Module 6 Guideline; "*Earthquake Resistant Retaining Wall Design"* [34] and the NZ Structural Engineering Society's Guideline; "*Concrete Cantilever Retaining Walls*" [35]. The author thanks Dr Kevin McMannus, Mr Geoff Bird and Mr Allan McPherson for very informative discussions during this work.

LimitState provided a complimentary license to use LS: Geo (https://www.limitstate.com/geo) for research.

The paper was greatly improved by incorporating the corrections and suggestions made by one of the unnamed Reviewers.

REFERENCES

1 Mononobe N and Matsuo H (1929). "On the determination of earth pressures during earthquakes". *Proceedings of the World Engineering Congress*, **9**: 177-185.

2 Wood JH (1973). "*Earthquake-induced Soil Pressures on Structures"*. Report EERL 73-05. California Institute of Technology, Pasadena, 309pp.

3 Wood JH (2019). "Earthquake design of flexible soil-retaining structures". *Proceedings of the Institution of Civil Engineers – Geotechnical Engineering*, **172**(1): 12pp. https://doi.org/10.1680/jgeen.17.00192

4 Smith CC and Cubrinovski M (2011). "Pseudo-static limit analysis by discontinuity layout optimization: Application to seismic analysis of retaining walls". *Soil Dynamics and Earthquake Engineering*, **31**(10): 1311-1323. https://doi.org/10.1016/j.soildyn.2011.03.014

5 Mikola RG and Sitar N (2013). *"Seismic Earth Pressures on Retaining Structures in Cohesionless Soil"*. Report No UCB GT 13-01. Department of Civil and Environmental Engineering, University of California, Berkley, 170pp.

6 FLAC, Itasca International, Inc. https://www.itascainternational.com/

7 Koseki J, Tatsuoka F, Munaf Y, Tateyama M and Kojima K (1998). "A modified procedure to evaluate active earth pressure at high seismic loads". *Special Issue of Soils and Foundations*, 209-216. https://doi.org/10.3208/sandf.38.Special_209

8 Bolton MD and Steedman RS (1985). "Modelling the seismic resistance of retaining structures". *Proceedings of the 11th International Conference on Soil Mechanics and Foundation Engineering*, **4**: 1845-1848.

9 Watanabe K, Koseki J and Tateyama M (2011). "Seismic pressures exerted on retaining walls under a large seismic load". *Soils and Foundations*, **51**(3): 379–394. https://doi.org/10.3208/sandf.51.379

10 Shukla SK (2015). "Generalized analytical expression for dynamic active thrust from c-ϕ soil backfills". *International Journal of Geotechnical Engineering*, **9**(4): 416-421. https://doi.org/10.1179/1939787914Y.0000000076

11 Shukla SK (2013). "Generalized analytical expression for dynamic passive earth pressure from c-ϕ soil backfills". *International Journal of Geotechnical Engineering*, **7**(4): 443-446. http://dx.doi.org/10.1179/1939787913Y.0000000001

12 Terzaghi K, Peck RB and Mesri G (1996). "*Soil Mechanics in Engineering Practice*". Wiley & Sons, New York, 592pp.

13 Newmark NM (1965). "Effects of earthquakes on dams and embankments". *Geotechnique*, **XV**(2): 139-157. https://doi.org/10.1680/geot.1965.15.2.139

14 Jibson RW (2007). "Regression models for estimating coseismic landslide displacement". *Engineering Geology*, **91**(2-4): 209-218. http://dx.doi.org/10.1016/j.enggeo.2007.01.013

15 Ambraseys NN and Menu JM (1988). "Earthquake–induced ground displacements". *Earthquake Engineering and Structural Dynamics*, **16**: 985-006. https://doi.org/10.1002/eqe.4290160704

16 Ambraseys N and Srbulov M (1995). "Earthquake-induced displacements of slopes". *Soil Dynamics and Earthquake Engineering*, **14**: 59-71. https://doi.org/10.1016/0267-7261(94)00020-H

17 Anderson DG, Martin GR, Lam I and Wang JN (2008). "*Seismic Analysis and Design of Retaining Walls, Buried Structures, Slopes and Embankments"*. NCHRP Report 611, Transportation Research Board, 137pp.

18 Bray JD, Travasarou T and Zupan J (2010). "Seismic displacement design of earth retaining structures". *ASCE, Earth Retention Conference*, (ER2010), Washington, 638-655. http://dx.doi.org/10.1061/41128(384)65

19 Lai CS (1979). *"Behaviour of Retaining Walls under Seismic Loading"*. Report 79-9, Department of Civil Engineering, University of Canterbury, Christchurch, NZ, 108pp.

20 Lai CS and Berrill JB (1979). "Shaking table tests on a model retaining wall". *Bulletin of the NZ National Society for Earthquake Engineering*, **12** (2): 122-126. https://doi.org/10.5459/bnzsee.12.2.122-126

21 Wood JH and Elms DG (1990). "Seismic design of bridge abutments and retaining walls". *Bridge Design and Research Seminar*. Vol 2: RRU Bulletin 84. Transit NZ, Wellington, 90pp.

22 Matsuzawa H, Ishibashi I and Kawamura M (1985). "Dynamic soil and water pressures". *ASCE Journal of Geotechnical Engineering*. **11**(10): 1161-1176. https://doi.org/10.1061/%28ASCE%290733-9410%281985%29111%3A10%281161%29

23 Westergaard HM (1933). "Water pressures on dams during earthquakes". *Transactions of ASCE*, **98**(2): 418-433. https://doi.org/10.1061/TACEAT.0004496

24 Kramer SL (1996). *"Geotechnical Earthquake Engineering"*. Prentice Hall, New Jersey, 653pp.

25 Standards New Zealand (2004). "*NZS1170.5: Structural Design Actions. Part 5: Earthquake Actions - New Zealand*". Standards New Zealand, Wellington, NZ, 76pp. https://www.standards.govt.nz/sponsored-standards/building-standards/NZS1170-5

26 Choudhury D (2004). "Seismic passive resistance at soil-wall interface". *13th World Conference on Earthquake Engineering*, Vancouver. Paper No 2746, 8pp.

27 Kumar J (2001). "Dynamic passive earth pressure coefficients for sands". *Canadian Geotechnical Journal*, **38**: 876-881. http://www.nrcresearchpress.com/doi/abs/10.1139/t01-004

28 Morrison EE and Ebling RM (1995). "Limit equilibrium computation of dynamic earth pressure". *Canadian Geotechnical Journal*, **32**: 481-487. https://doi.org/10.1139/t95-050

29 Mylonakis G, Kloukinas P and Papantonopoulos C (2007). "An alternative to the Mononobe–Okabe equations for seismic earth pressures". *Soil Dynamics and Earthquake Engineering*, **27**: 957-969. https://doi.org/10.1016/j.soildyn.2007.01.004

30 Soubra AH (2000). "Static and seismic passive earth pressure coefficients on rigid retaining structures". *Canadian Geotechnical Journal*, **37**: 463-478. https://doi.org/10.1139/t99-117

31 Subba Rao KS and Choudhury D (2005). "Seismic passive earth pressure in soils". *ASCE Journal of Geotechnical Engineering*, **113**(1): 131-135. https://doi.org/10.1061/(ASCE)1090-0241(2005)131:1(131)

32 Jacobsen PN (1980). *"Translational Behaviour of Gravity Retaining Walls during Earthquakes"*. Report No 80-9, Department of Civil Engineering, University of Canterbury, Christchurch, NZ, 123pp.

33 Aitken GH (1982). *"Seismic Response of Retaining Walls"*. Report. No 82-5, Department of Civil Engineering, University of Canterbury, Christchurch, NZ, 87pp.

34 NZGS (2021). *"Earthquake Geotechnical Engineering Practice: Module 6. Earthquake Resistant Retaining Wall Design"*. New Zealand Geotechnical Society (NZGS), Wellington, NZ, 70pp. https://www.nzgs.org/

35 SESOC (2021). *"Simplified Structural Design Guide: Concrete Cantilever Retaining Walls"*. Draft for review, Authors: AR McPherson, and GD Bird. Structural Engineering Society New Zealand (SESOC), 50pp. https://www.sesoc.org.nz.